



Deposited via The University of Sheffield.

White Rose Research Online URL for this paper:

<https://eprints.whiterose.ac.uk/id/eprint/112609/>

Version: Accepted Version

---

**Article:**

Olumayegun, O., Wang, M. and Kelsall, G. (2017) Thermodynamic analysis and preliminary design of closed Brayton cycle using nitrogen as working fluid and coupled to small modular Sodium-cooled fast reactor (SM-SFR). *Applied Energy*, 191. pp. 436-453. ISSN: 0306-2619

<https://doi.org/10.1016/j.apenergy.2017.01.099>

---

**Reuse**

Items deposited in White Rose Research Online are protected by copyright, with all rights reserved unless indicated otherwise. They may be downloaded and/or printed for private study, or other acts as permitted by national copyright laws. The publisher or other rights holders may allow further reproduction and re-use of the full text version. This is indicated by the licence information on the White Rose Research Online record for the item.

**Takedown**

If you consider content in White Rose Research Online to be in breach of UK law, please notify us by emailing [eprints@whiterose.ac.uk](mailto:eprints@whiterose.ac.uk) including the URL of the record and the reason for the withdrawal request.

# 1 Thermodynamic Analysis and Preliminary Design of 2 Closed Brayton Cycle Using Nitrogen as Working Fluid 3 and Coupled to Small Modular Sodium-cooled Fast 4 Reactor (SM-SFR) 5

6 **Olumide Olumayegun<sup>a</sup>, Meihong Wang<sup>a</sup>, Greg Kelsall<sup>b</sup>**

7 <sup>a</sup> Process and Energy Systems Engineering Group, School of Engineering, University of Hull,  
8 Cottingham Road, Hull, HU6 7RX, United Kingdom

9 <sup>b</sup> GE Power, Newbold Road, Rugby, CV21 2NH, Warwickshire, United Kingdom  
10

## 11 **Abstract**

12 Sodium-cooled fast reactor (SFR) is considered the most promising of the Generation IV  
13 reactors for their near-term demonstration of power generation. Small modular SFRs (SM-  
14 SFRs) have less investment risk, can be deployed more quickly, are easier to operate and are  
15 more flexible in comparison to large nuclear reactor. Currently, SFRs use the proven Rankine  
16 steam cycle as the power conversion system. However, a key challenge is to prevent dangerous  
17 sodium-water reaction that could happen in SFR coupled to steam cycle. Nitrogen gas is inert  
18 and does not react with sodium. Hence, intercooled closed Brayton cycle (CBC) using nitrogen  
19 as working fluid and with a single shaft configuration has been one common power conversion  
20 system option for possible near-term demonstration of SFR. In this work, a new two shaft  
21 nitrogen CBC with parallel turbines was proposed to further simplify the design of the  
22 turbomachinery and reduce turbomachinery size without compromising the cycle efficiency.  
23 Furthermore, thermodynamic performance analysis and preliminary design of components  
24 were carried out in comparison with a reference single shaft nitrogen cycle. Mathematical  
25 models in Matlab were developed for steady state thermodynamic analysis of the cycles and  
26 for preliminary design of the heat exchangers, turbines and compressors. Studies were  
27 performed to investigate the impact of the recuperator minimum terminal temperature  
28 difference (TTD) on the overall cycle efficiency and recuperator size. The effect of  
29 turbomachinery efficiencies on the overall cycle efficiency was examined. The results showed  
30 that the cycle efficiency of the proposed configuration was comparable to the 39.44%  
31 efficiency of the reference cycle. In addition, the study indicated that the new configuration  
32 has the potential to simplify the design of turbomachinery, reduce the size of turbomachinery  
33 and provide opportunity for improving the efficiency of the turbomachinery. The findings so  
34 far revealed that the proposed two-shaft CBC with nitrogen as working fluid could be a  
35 promising power conversion system for SM-SFRs near-term demonstration.  
36

## 37 **Keywords**

38 Sodium-cooled fast reactor

39 Closed Brayton cycle

40 Nitrogen working fluid

41 Thermodynamic analysis

42 Heat exchanger design

43 Turbomachinery design

## 44 **Highlights**

- 45 • Nitrogen closed Brayton cycle for small modular sodium-cooled fast reactor studied
- 46 • Thermodynamic modelling and analysis of closed Brayton cycle performed
- 47 • Two-shaft configuration proposed and performance compared to single shaft
- 48 • Preliminary design of heat exchangers and turbomachinery carried out

## 49 **Nomenclature and Units**

### 50 **Abbreviations**

|                       |  |
|-----------------------|--|
| 2-D                   | Two-dimensional  |
| ASTRID                | Advanced Sodium Technological Reactor for Industrial Demonstration |
| CBC                   | closed Brayton cycle   |
| CDT                   | compressor-driving turbine   |
| FPT                   | free power turbine   |
| Gen IV                | Generation IV  |
| GIF                   | Gen IV International Forum   |
| HPC                   | high pressure compressor   |
| IHX                   | intermediate heat exchanger  |
| LMTD                  | logarithmic mean temperature difference                            |
| LPC                   | low pressure compressor  |
| Na/N <sub>2</sub> IHX | sodium/nitrogen intermediate heat exchanger                        |
| NIST                  | National Institute of Standards and Technology                     |
| PCHE                  | Printed Circuit Heat Exchanger                                     |
| PCS                   | power conversion system  |
| s-CO <sub>2</sub>     | supercritical carbon dioxide                                       |
| SFR                   | sodium-cooled fast reactor   |
| SM-SFR                | small modular sodium-cooled fast reactor                           |
| SMR                   | small modular reactor  |
| TTD                   | terminal temperature difference                                    |

51

### 52 **Symbols**

|           |  |
|-----------|--|
| $A$       | Area (m <sup>2</sup> )                         |
| $AR$      | Aspect ratio                                   |
| $b_H$     | Blade height (m)                               |
| $c$       | Blade chord (m)                                |
| $C$       | Absolute velocity (m/s)                        |
| $C_L$     | Lift coefficient                               |
| $C_p$     | Specific heat capacity at constant pressure    |
| $D$       | Diameter (m)                                   |
| $DF$      | Diffusion factor                               |
| $dHaller$ | de Haller number                               |
| $d_s$     | Specific diameter                              |
| $f$       | Darcy friction factor                          |
| $g$       | Gravitational acceleration (m/s <sup>2</sup> ) |

|               |   |
|---------------|---|
| $H$           | Head (m)  |
| $h$           | Specific enthalpy (kJ/kg) or convective heat transfer coefficient [W/(m <sup>2</sup> .K)] |
| $k$           | Thermal conductivity [W/(m.K)]  |
| $L$           | Length (m)  |
| $\ln$         | Natural logarithm   |
| $\dot{m}$     | Mass flow rate (kg/s)   |
| $\min$        | Minimum   |
| $n_s$         | Specific speed  |
| $N_b$         | Number of blade   |
| $Nu$          | Nusselt number  |
| $op$          | Optimum value   |
| $P$           | Pressure (Pa or N/m <sup>2</sup> )  |
| $Pr$          | Prandtl Number  |
| $\dot{Q}$     | Volumetric flow rate (m <sup>3</sup> /s)  |
| $Q$           | Heat duty (watt or J/s)   |
| $r$           | Radius (m)  |
| $Re$          | Reynold number  |
| $s$           | Blade spacing (m)   |
| $T$           | Temperature (K)   |
| $t$           | Conduction length (m)   |
| $U$           | Overall heat transfer coefficient [W/(m <sup>2</sup> .K)] or blade velocity (m/s)         |
| $V$           | Velocity (m/s)  |
| $W$           | Power (W or J/s) or relative velocity (m/s)   |
| $\alpha$      | Absolute velocity angle (degree)  |
| $\beta$       | Relative velocity angle (degree)  |
| $\Delta$      | Change in quantity  |
| $\delta$      | Fluid deflection through blade  |
| $\varepsilon$ | Effectiveness or pipe roughness   |
| $\eta$        | Efficiency  |
| $\Lambda$     | Reaction  |
| $\mu$         | Viscosity (Pa-s)  |
| $\xi$         | Relative pressure loss or blade nominal loss coefficient                                  |
| $\pi$         | Pressure ratio or pi  |
| $\rho$        | Density (kg/m <sup>3</sup> )  |
| $\sigma$      | Blade solidity  |
| $\phi$        | Flow coefficient  |
| $\psi$        | Stage loading coefficient   |
| $\omega$      | Rotational speed (rev/s)  |

53

## 54 Subscripts

|        |  |
|--------|--|
| 0      | Stagnation property                      |
| 1      | Turbine or compressor stage inlet        |
| 2      | Turbine rotor or compressor stator inlet |
| 3      | Turbine or compressor stage exit         |
| $ad$   | adiabatic                                |
| $C$    | Compressor                               |
| $c$    | Cold stream                              |
| $elec$ | Electrical                               |
| $ex$   | Exit                                     |
| $gen$  | Generator                                |

|                      |                         |
|----------------------|-------------------------|
| <i>h</i>             | Hot stream or hydraulic |
| <i>HX</i>            | Heat exchanger          |
| <i>i</i>             | inlet                   |
| <i>is</i>            | Isentropic              |
| <i>N<sub>2</sub></i> | Nitrogen                |
| <i>Na</i>            | Sodium                  |
| <i>m</i>             | Melting or mean-line    |
| <i>max</i>           | Maximum                 |
| <i>o</i>             | Outlet                  |
| <i>P</i>             | Pump                    |
| <i>RX</i>            | Reactor                 |
| <i>T</i>             | Turbine or Temperature  |
| <i>tt</i>            | Total-to-total          |
| <i>x</i>             | Axial component         |
| <i>θ</i>             | Tangential component    |

55

## 56 **1 Introduction**

57 Generation IV nuclear reactors (Gen IV reactors) are the next step in the deployment of nuclear  
58 power generation to meet the world's future energy demand [1]. Of all the six Gen IV reactors,  
59 sodium-cooled fast reactor (SFR) has been identified as the most matured and hence the most  
60 suitable for near-term demonstration [2-4]. In addition to the larger SFRs, Small Modular  
61 Sodium-cooled Fast Reactors (SM-SFRs) with plant size ranging from 50 to 300 MWe are  
62 also under consideration by Gen IV International Forum (GIF) [5]. Generally, small modular  
63 reactors (SMRs) are viewed to have less financial risk, cheaper when mass produced, could be  
64 deployed faster, and are easier to operate and maintain compared with larger nuclear reactor  
65 [6, 7]. Most of the components could be factory-built and then assemble on site. In addition,  
66 SMRs are more flexible with respect to their generation and location due to their lower  
67 capacity. Therefore, SMRs could help cope with the challenge of intermittent renewable  
68 energy by rapidly increasing or decreasing power output [8-11]. Also, it can be sited in off-  
69 grid areas requiring small power and future growth can be accommodated by simply adding  
70 extra units.

71 The power conversion system (PCS) implementation is critical to the successful  
72 commercialization of the SM-SFR power plant technology. The current SFRs (e.g. Phenix,  
73 SuperPhenix, BN 600, BN 800, e.t.c.) adopt the proven Rankine steam cycle as PCS [12, 13].  
74 However, there are concerns over the coupling of steam cycle to SFR. The challenges include:  
75 (1) safety concern because of the possibility of hazardous sodium-water reaction (2) high  
76 capital cost because of additional secondary sodium circuit and large plant footprint, and (3)  
77 low efficiency. Therefore, closed Brayton cycle (CBC) is considered as a promising alternative  
78 PCS for SFRs. Recently, Olumayegun et al carried out a review of the research activities and  
79 studies performed worldwide on CBC [14]. Use of CBC has the potential to simplify the design,  
80 reduce technical risk, reduce the amount and size of equipment and improve efficiency.  
81 Working fluids consider for the CBC include supercritical CO<sub>2</sub> (s-CO<sub>2</sub>), helium and nitrogen.

82 In 1966, Feher patented the supercritical cycle heat engine and the possibility of using s-CO<sub>2</sub>  
83 cycle for nuclear power generation was later investigated [14, 15]. Recent times has witnessed  
84 a renewed interest in s-CO<sub>2</sub> cycle [16] as PCS for nuclear power [17-19] and other heat sources  
85 such as concentrated solar power [20-22], fuel cell [23], coal [24] and waste heat[25]. In  
86 literature, s-CO<sub>2</sub> cycle has been investigated as alternative to steam cycle for SFR application  
87 [3, 26-32]. All the studies agreed on the benefits of s-CO<sub>2</sub> CBC power conversion system for  
88 SFR including higher efficiency (about 44%) and smaller footprint. However, sodium-CO<sub>2</sub>  
89 reaction could be of safety concern at some temperatures and requires further investigation to

90 understand the nature of the chemical reaction [29, 33]. Also, s-CO<sub>2</sub> CBC still requires major  
91 technological developments for the turbomachinery and heat exchangers [3, 29]. Helium gas  
92 does not react with sodium but helium CBC is not promising for SFRs due to its low thermal  
93 efficiency [12]. The nitrogen CBC option is attractive because nitrogen is inert, thus  
94 eliminating the risk of sodium-water or sodium-CO<sub>2</sub> reactions. Furthermore, design of  
95 nitrogen PCS is anticipated to be less challenging since years of experience from air gas turbine  
96 engines can be applied [34]. After all, nitrogen properties are similar to those of air. Hence,  
97 the nitrogen cycle was perceived as the only potential option for short-term demonstration  
98 while the s-CO<sub>2</sub> cycle could be a suitable option for long-term applications [12, 35].

99 The nitrogen gas Brayton cycle is mainly been developed in France under the ASTRID  
100 (Advanced Sodium Technological Reactor for Industrial Demonstration) SFR project [35-37].  
101 Cachon et al. [37] presented different feasibility studies and heat exchanger design for  
102 innovative power conversion systems for ASTRID SFR. The result led to the selection of  
103 nitrogen gas Brayton cycle. Alpy et al. [35] performed a comparison in terms of the  
104 thermodynamic performance and preliminary components sizing between nitrogen and s-CO<sub>2</sub>  
105 cycle for the ASTRID SFR. The s-CO<sub>2</sub> cycle has a higher efficiency (about 44%) than the  
106 nitrogen cycle (about 38%). However, the nitrogen cycle was chosen for near-term  
107 demonstration of electricity generation from CBC coupled to SFR. Ahn and Lee investigated  
108 several CBC designs for SM-SFR as alternatives to the Rankine steam cycle [7]. CBC using  
109 s-CO<sub>2</sub>, helium and nitrogen as working fluids was compared in term of thermodynamic  
110 performance and physical size of the components. Recently, Seo et al. [13] investigated the  
111 adoption of nitrogen power conversion system for a SM-SFR. Nitrogen working fluid was  
112 chosen ahead of s-CO<sub>2</sub> and helium considering both safety and thermal performance as well  
113 as the elimination of intermediate sodium loop. Sensitivity studies were performed to optimise  
114 the system and the effect of the elimination of intermediate (secondary) sodium loop on the  
115 thermodynamic efficiency of the plant was studied. The study showed that the elimination of  
116 the intermediate loop increased the thermodynamic efficiency by 3% point.

117 The aim of this paper is the thermodynamic analysis and preliminary design of components of  
118 CBC using nitrogen as working fluid and coupled to SM-SFR for near-term demonstration of  
119 electricity generation from Gen IV reactors. The often suggested configuration for the nitrogen  
120 cycle is the intercooled CBC with single shaft, in which all the compressors, turbine and  
121 generator rotates at the grid frequency. However, preliminary design of the turbomachinery  
122 indicated that the design of the turbine is especially difficult [38]. One solution for simplifying  
123 and improving the design of turbomachinery is to change the shaft rotational speed. This  
124 requires the use of either frequency converter or gearbox, both of which will incur efficiency  
125 penalty. Moreover, maximum practical power output for which a gearbox is feasible is about  
126 80 MW [39]. Another option is to employ a two-shaft configuration in which the generator  
127 and a free power turbine (FPT) rotate at the grid frequency while the compressors and a  
128 compressor-driving turbine (CDT) rotate at an independent shaft speed. The free selection of  
129 a higher compressors shaft speed can then be used to optimise the design of the compressors  
130 and the driving turbine. This will result in reduced stage numbers and more compact  
131 turbomachinery as well as possible improvement of turbomachinery efficiency. Two layouts  
132 are possible for the two-shaft configuration. One is to have the FPT and the CDT in series and  
133 the other is to have them in parallel. The two-shaft with parallel turbines layout is adopted in  
134 this study as the series turbines layout is known to result in loss of overall cycle efficiency  
135 [40].

136 To the best of our knowledge, no one has investigated a two-shaft configuration option for  
137 nitrogen cycle coupled to SFR. Also, most previous studies of CBC tend to be limited to  
138 thermodynamic performance analysis [3, 6, 13]. In summary, the main novel contributions of  
139 this article are: (a) a new two-shaft nitrogen CBC with parallel turbines was proposed as a way  
140 to further simplify the design of the turbomachinery and reduce turbomachinery size without

141 compromising the cycle efficiency (b) thermodynamic performance analysis were carried out  
142 in comparison with a reference single shaft nitrogen cycle (c) preliminary design of  
143 components were performed for the proposed and the reference configurations. Further effort  
144 in this work to estimate the sizes of components through preliminary design can be crucial to  
145 the economic assessment of the plants. The effect of the recuperator minimum terminal  
146 temperature difference (TTD) on the cycle efficiency and recuperator size was investigated.  
147 The impact of changes in turbomachinery efficiency on the overall cycle efficiency was  
148 examined. The thermodynamic performances and preliminary designs were evaluated using  
149 the Matlab codes developed for cycle analysis, heat exchanger design, axial compressor design  
150 and axial turbine design. The performance calculation and preliminary design were performed  
151 for nitrogen Brayton cycles coupled to a SFR with thermal power of 500 MW and reactor exit  
152 temperature of 545 °C.

153 The structure of the paper is as follows. Section 2 describes the layout of the reference single-  
154 shaft and the proposed two-shaft with parallel turbines configuration. Section 3 outlines the  
155 methodology for cycle thermodynamic modelling and performance analysis. In Section 4 the  
156 methodology for the preliminary design of the heat exchangers and turbomachinery is  
157 presented. Section 5 presents the results and discussion of the thermodynamic analysis and  
158 preliminary design for the nitrogen cycles. Finally, conclusions are drawn in Section 7.

## 159 **2 Plant configurations and description**

160 In this study, two nitrogen CBC configurations have been considered: a reference single-shaft  
161 intercooled closed-cycle gas turbine configuration and a two-shaft with parallel turbines  
162 configuration. The single-shaft intercooled configuration seems to be the most popular design  
163 choice for nitrogen CBC. Hence it will be used as reference case for comparison with the  
164 suggested alternative two-shaft configuration. A more detailed description of the two  
165 configurations will be presented in this section.

### 166 **2.1 Reference single-shaft intercooled closed Brayton cycle**

167 The schematic flow diagram of the reference single-shaft intercooled CBC is shown in Figure  
168 1. In this configuration, all the turbomachinery rotates on a single shaft. The plant features a  
169 500 MWth SFR coupled indirectly to the PCS through the sodium/nitrogen intermediate heat  
170 exchanger (Na/N<sub>2</sub> IHX). The primary circuit is made up of the SFR reactor, the primary side  
171 of Na/N<sub>2</sub> IHX and the sodium pump. Sodium coolant at 545 °C and 1.15 bar exits the reactor  
172 core and flows through the primary side of the IHX. The pump is used to circulate the liquid  
173 sodium in the primary circuit. Thus the reactor core heat is transferred to the PCS via the Na/N<sub>2</sub>  
174 IHX. The PCS is connected to the secondary side of the Na/N<sub>2</sub> IHX and uses nitrogen as  
175 working fluid. The Brayton cycle consists of two compressors referred to as low pressure  
176 compressor (LPC) and high pressure compressor (HPC), a turbine and four heat exchangers  
177 (Na/N<sub>2</sub> IHX, recuperator, precooler and intercooler).

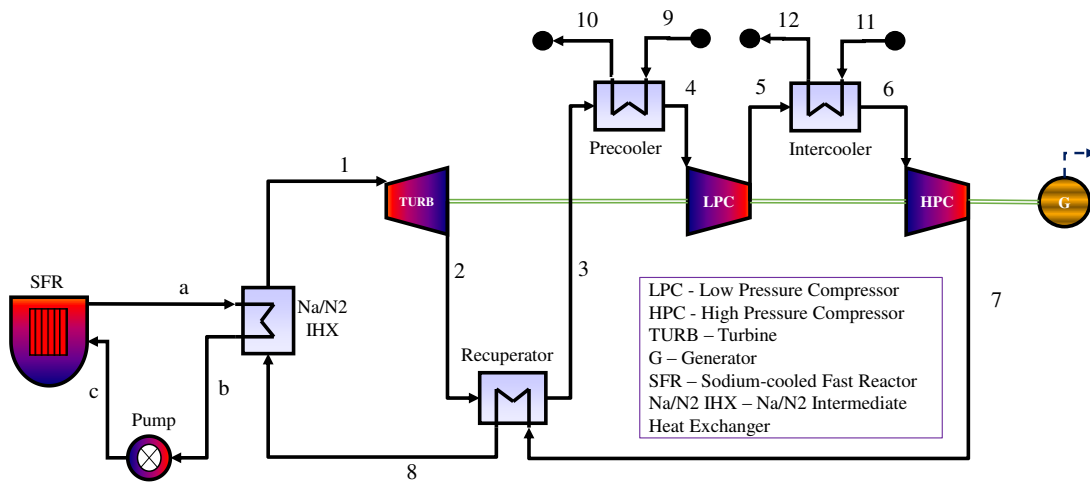
178 The temperature-entropy (T-S) diagram of the closed Brayton PCS is illustrated in Figure 2.  
179 High temperature nitrogen leaving the Na/N<sub>2</sub> IHX at 530 °C is expanded in the turbine to  
180 produce mechanical power. The power produced by the turbine is used to drive the electrical  
181 generator, the LPC and the HPC connected to the same shaft. The shaft rotates at the grid  
182 synchronous speed of 3000 rpm since the generator is directly connected to the grid. Part of  
183 the residual heat energy in the low pressure nitrogen exiting the turbine is recovered in the  
184 recuperator. The nitrogen gas then enters the precooler where the remaining heat energy is  
185 rejected to the surrounding through the cooling water. The cooled nitrogen at 27 °C is  
186 compressed in the LPC, cooled again in the intercooler to 27 °C and compressed to the  
187 maximum cycle pressure of 180 bar by the HPC. It then enters the high pressure side of the  
188 recuperator where it is preheated with the heat energy recovered from the fluid leaving the  
189 turbine. After recuperation, the fluid passes through the secondary side of the Na/N<sub>2</sub> IHX. At

190 the outlet of the Na/N<sub>2</sub> IHX the nitrogen gas achieves the highest temperature within the cycle  
 191 after absorbing heat from liquid sodium flowing through the primary side. The hot nitrogen gas  
 192 is then routed to the turbine to repeat the thermodynamic cycle.

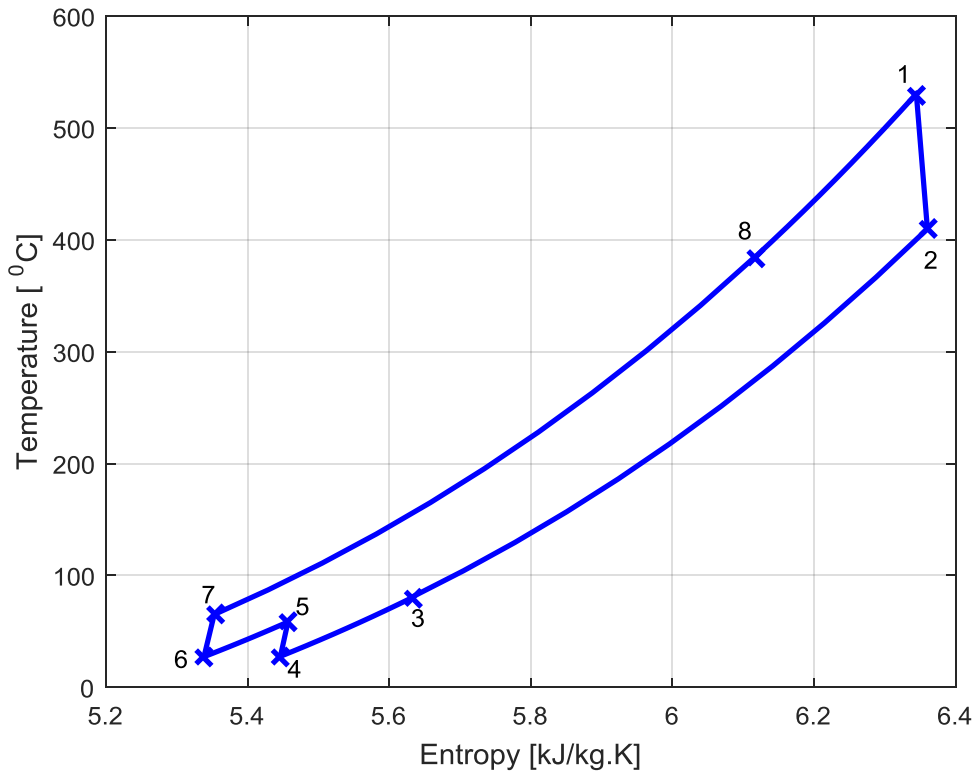
## 193 2.2 Two-shaft with parallel turbines closed Brayton cycle

194 The schematic diagram of the proposed alternative two-shaft configuration is shown in Figure  
 195 3. It is similar to the reference case except that (a) it uses two parallel turbines referred to as  
 196 compressor-driving turbine (CDT) and free power turbine (FPT), and (b) it employs two  
 197 independent rotor shafts referred to as compressor shaft and generator shaft. The CDT drives  
 198 the LPC and the HPC through the compressor shaft while the FPT drives the electrical  
 199 generator through the generator shaft. The main nitrogen flow exiting the Na/N<sub>2</sub> IHX is split  
 200 into two streams at the turbines inlet. The first stream is expanded in the CDT rotating at speed  
 201 higher than 3000rpm. The flow through this turbine is just enough to drive the LPC and the  
 202 HPC. The second stream flow through the FPT rotating at 3000 rpm to match the grid  
 203 frequency and generate electric power.

204 A significant feature of the two-shaft parallel turbines configuration is that the compressor  
 205 shaft speed can be selected to minimise the technical design challenges of the turbomachines  
 206 as their design could be optimised for non-grid rotational speed. Also the use of two parallel  
 207 turbines instead of series arrangement helps to maintain the thermal efficiency of the PCS [40]  
 208 as well as reduce the volumetric flow through the turbines.

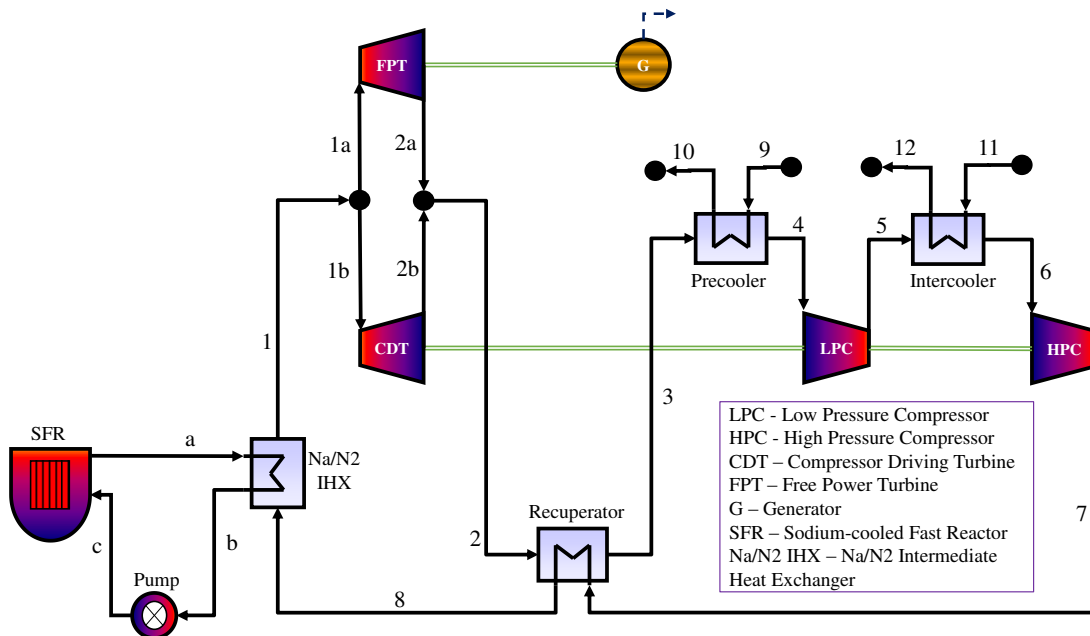


209  
 210 *Figure 1 Reference single-shaft closed Brayton cycle [7, 35]*



211

212 *Figure 2 Temperature-Entropy diagram*



213

214 *Figure 3 Proposed two-shaft closed Brayton cycle with turbines in parallel*

## 215 **3 Thermodynamic analysis and cycle modelling**

### 216 **3.1 Thermodynamic modelling of cycle components and** 217 **performance evaluation**

218 Using Matlab, a cycle analysis code was developed for CBC coupled to SFR. Steady state  
219 thermodynamic performance of the nitrogen CBC was evaluated with the Matlab code. The  
220 cycle calculation code consists of models of the SFR reactor, pump, IHX, recuperator,  
221 precooler, intercooler, compressors, turbines and pipes. Models of the individual component  
222 were derived based on steady state mass and energy balances, thermodynamic relations and  
223 characteristic equations of the components.

224 Assumed known were: reactor thermal power; core outlet temperature and pressure; cycle  
225 maximum pressure; hot side outlet temperatures of intermediate heat exchanger (IHX),  
226 precooler and intercooler; turbomachinery isentropic efficiencies; minimum TTD or  
227 effectiveness of heat exchangers; generator efficiency; and relative pressure losses of pipes  
228 and heat exchangers. Consequently, the mass flows, fluid thermodynamic states, heat  
229 transferred, mechanical power delivered or absorbed, generator output and cycle efficiency  
230 were evaluated. The whole cycle calculation process begins with initial guesses for the LPC  
231 and HPC pressure ratios. The iteration is continued until optimum values of compressor ratios  
232 in term of the maximum cycle efficiency are obtained. Note that any thermodynamic property  
233 can be obtained from the fluid thermodynamic property sources if two independent properties  
234 are known.

235 The reactor was modelled as a heat source. For the given reactor thermal power, the primary  
236 circuit sodium mass flow rate was calculated using equation (1)

$$Q_{RX} = \dot{m}_{Na}(h_{RXo} - h_{RXi}) \quad (1)$$

237 Where,

238  $Q_{RX}$  is reactor thermal power  
239  $\dot{m}_{Na}$  is the mass flow rate of sodium coolant  
240  $h_{RXo}$  is the specific enthalpy of sodium at reactor outlet  
241  $h_{RXi}$  is the specific enthalpy of sodium at reactor inlet

242 The liquid sodium is recycled by the pump. The external power input in the pump is given as:

$$W_p = \dot{m}_{Na}(h_{Po} - h_{Pi}) \quad (2)$$

243 Where,

244  $W_p$  is pump power  
245  $h_{Po}$  is the specific enthalpy at pump outlet  
246  $h_{Pi}$  is the specific enthalpy at pump inlet

247 The pump isentropic efficiency is:

$$\eta_{p,is} = \frac{h_{Po,is} - h_{Pi}}{h_{Po} - h_{Pi}} \quad (3)$$

248 Where,

249  $\eta_{p,is}$  is the pump isentropic efficiency  
250  $h_{Po,is}$  is the ideal specific enthalpy at pump outlet with isentropic pressure rise

251 For an isentropic process in the pump, it follows that the first law for closed system undergoing  
252 reversible process becomes:

$$h_{P_{O,IS}} - h_{P_i} = \frac{P_{P_o} - P_{P_i}}{\rho_{P_i}} \quad (4)$$

253 Where,

254  $P_{P_o}$  is the pump outlet pressure

255  $P_{P_i}$  is the pump inlet pressure

256  $\rho_{P_i}$  is the density of sodium at pump inlet

257 The compressors were modelled using their pressure ratios and isentropic efficiencies. The  
258 compressor outlet conditions were computed from equation (5) and (6):

$$P_{C_o} = P_{C_i}\pi \quad (5)$$

259 Where,

260  $P_{C_o}$  is the compressor outlet pressure

261  $P_{C_i}$  is the compressor inlet pressure

262  $\pi$  is the pressure ratio

$$\eta_{C,IS} = \frac{h_{C_o,IS} - h_{C_i}}{h_{C_o} - h_{C_i}} \quad (6)$$

263 Where,

264  $\eta_{C,IS}$  is the isentropic efficiency of the compressor

265  $h_{C_o,IS}$  is the ideal specific enthalpy at compressor outlet with isentropic compression

266  $h_{C_i}$  is the specific enthalpy at compressor inlet

267  $h_{C_o}$  is the specific enthalpy at compressor outlet

268 The power consumption of the compressors,  $W_C$  is calculated as the product of nitrogen mass  
269 flow,  $\dot{m}_{N_2}$  and enthalpy rise between the inlet and outlet of the compressors.

$$W_C = \dot{m}_{N_2}(h_{C_o} - h_{C_i}) \quad (7)$$

270

271 Similarly, the turbines were modelled using the pressure ratios and isentropic efficiencies. The  
272 pressure, enthalpy and power were calculated by using equation (8), (9) and (10).

$$P_{T_o} = \frac{P_{T_i}}{\pi} \quad (8)$$

273 Where,

274  $P_{T_o}$  is the turbine outlet pressure

275  $P_{T_i}$  is the turbine inlet pressure

$$\eta_{T,IS} = \frac{h_{T_i} - h_{T_o}}{h_{T_i} - h_{T_o,IS}} \quad (9)$$

276 Where,

277  $\eta_{T,IS}$  is the isentropic efficiency of the turbine

278  $h_{T_o,IS}$  is the ideal specific enthalpy at turbine outlet with isentropic expansion

279  $h_{T_i}$  is the specific enthalpy at turbine inlet

280  $h_{T_o}$  is the specific enthalpy at turbine outlet

$$W_T = \dot{m}_{N_2}(h_{T_i} - h_{T_o}) \quad (10)$$

281 Where  $W_T$  is the power delivered by the turbine

282 The IHX, recuperator, precooler and intercooler were modelled as counter flow heat  
283 exchangers. Two calculation options are available. The first option is to assume that the

284 minimum TTD is known while the second option is to assume that the effectiveness is known.  
 285 Using the TTD approach, the minimum TTD can occur either at the hot end (hot stream  
 286 inlet/cold stream outlet) or at the cold end (cold stream inlet/hot stream outlet). As an initial  
 287 guess, the TTD was assumed to occur at the hot end, then:

$$T_{co} = T_{hi} - TTD \quad (11)$$

288 Where,

289  $T_{co}$  is the cold stream outlet temperature

290  $T_{hi}$  is the hot stream inlet temperature

291 Therefore, the heat exchanger duty (heat transferred),  $Q_{HX}$  is:

$$Q_{HX} = \dot{m}_c(h_{co} - h_{ci}) \quad (12)$$

292 Where,

293  $\dot{m}_c$  is the cold stream mass flow rate

294  $h_{co}$  is the cold stream outlet specific enthalpy

295  $h_{ci}$  is the cold stream inlet specific enthalpy

296

297 Then the hot stream outlet enthalpy is:

$$h_{ho} = h_{hi} - \frac{Q_{HX}}{\dot{m}_h} \quad (13)$$

298 Where,

299  $\dot{m}_h$  is the hot stream mass flow rate

300  $h_{ho}$  is the hot stream outlet specific enthalpy

301  $h_{hi}$  is the hot stream inlet specific enthalpy

302 If the temperature difference at cold end is discovered to be lower than the TTD, equation (11)  
 303 is replaced with equation (14). Then the above calculation is repeated but starting with cold  
 304 end.

$$T_{ho} = T_{ci} + TTD \quad (14)$$

305 Where,

306  $T_{ho}$  is the hot stream outlet temperature

307  $T_{ci}$  is the cold stream inlet temperature

308 However, if the effectiveness approach is to be used, the exchanger effectiveness,  $\varepsilon_{HX}$  is  
 309 defined as:

$$\varepsilon_{HX} = \frac{\dot{m}_c(h_{co} - h_{ci})}{Q_{max}} = \frac{\dot{m}_h(h_{hi} - h_{ho})}{Q_{max}} \quad (15)$$

310 The maximum theoretical heat transfer rate in counter flow heat exchanger of infinite heat  
 311 transfer surface area,  $Q_{max}$ , is given as follows:

$$Q_{max} = \min\{(\dot{m}_c(h_{coT_{hi}} - h_{ci})); (\dot{m}_h(h_{hi} - h_{hoT_{ci}}))\} \quad (16)$$

312 Where,

313  $h_{coT_{hi}}$  is the outlet enthalpy of cold stream at the temperature of the hot stream inlet

314  $h_{hoT_{ci}}$  is the outlet enthalpy of the hot stream at the cold stream inlet temperature

315 Inlet or outlet pressures of heat exchangers and pipes were calculated from the relative pressure  
 316 losses defined as:

$$\xi = \frac{P_i - P_o}{P_i} \quad (17)$$

317 Where,

318  $P_i$  is the inlet pressure

319  $P_o$  is the outlet pressure

320 The cycle thermodynamic states of pressure, temperature and enthalpy at all component inlet  
 321 and outlet were obtained by solving the equations (1) - (17). Then the electrical power supplied  
 322 to the grid,  $W_{elec}$  was calculated as:

$$W_{elec} = \eta_{gen} \left( \sum W_T - \sum W_C \right) - W_P \quad (18)$$

323 Where  $\eta_{gen}$  is the electrical generator efficiency

324 Note that pump power was not considered negligible in the cycle calculation. This will reduce  
 325 the plant efficiency. The cycle efficiency,  $\eta_{cycle}$  is defined as the ratio of electrical power  
 326 output to the reactor thermal power:

$$\eta_{cycle} = \frac{W_{elec}}{Q_{RX}} \quad (19)$$

327

328 The cycle analysis code is further integrated with the heat exchanger preliminary design  
 329 code/program. Heat exchanger design was performed based on the mass flows and fluid  
 330 conditions determined through the cycle calculation, and a chosen maximum pressure loss  
 331 constraint. Then the initial heat exchanger pressure losses used for cycle calculation is replaced  
 332 with the actual pressure losses obtained from the preliminary design code. The process is  
 333 repeated iteratively until there is convergence of the mass flows and fluid conditions. On the  
 334 other hand, the turbomachinery design code determined the number of stages and size of the  
 335 turbines and compressors.

### 336 3.2 Fluid thermodynamic and transport properties

337 The liquid sodium in the primary circuit carries the heat energy to be transferred to the PCS,  
 338 nitrogen gas is the working fluid in the PCS while liquid water in the cold side of the precooler  
 339 and intercooler is used for heat rejection to the environment. Hence the cycle analysis and the  
 340 preliminary design codes must be able to simulate the fluid properties of liquid sodium,  
 341 nitrogen gas and liquid water. Fluid thermodynamic properties to be simulated include:  
 342 pressure, temperature, enthalpy, density, heat capacity and speed of sound. Transport  
 343 properties include the dynamic viscosity and thermal conductivity.

344 Since Matlab does not have any thermodynamic and transport property function, a Matlab  
 345 code was written to compute the properties of liquid sodium. The computations were based on  
 346 correlations recommended by Sobolev [41]. A summary of the correlations used to generate  
 347 property values of liquid sodium is given in Table 1. The effect of pressure on the  
 348 thermodynamic and transport properties of liquid sodium was neglected. However, properties  
 349 of nitrogen and liquid water were obtained from REFPROP (version 9.1) program of the  
 350 National Institute of Standards and Technology (NIST). The REFPROP program has been  
 351 reported to be accurate and widely applicable to a variety of pure fluid and mixtures [42, 43].  
 352 Any unknown properties can be requested from the REFPROP program by supplying two  
 353 known independent properties. Both the Matlab code for liquid sodium property and the  
 354 REFPROP program were used as subroutines in the cycle analysis and preliminary design  
 355 codes.

356 **Table 1**  
 357 Correlations for computing liquid sodium properties

| Property               | Correlations (T is in Kelvins)   | Units             |
|------------------------|--|-------------------|
| Enthalpy               | $h = 164.8(T - T_m) - 1.97 \times 10^{-2}(T^2 - T_m^2) + 4.167 \times 10^{-4}(T^3 - T_m^3) + 4.56 \times 10^5(T^{-1} - T_m^{-1})$ ; $T_m = \text{melting temperature}$ | J/kg              |
| Density                | $\rho = 1014 - 0.235T$   | kg/m <sup>3</sup> |
| Specific heat capacity | $C_p = -3.001 \times 10^6 T^{-2} + 1658 - 0.8479T + 4.454 \times 10^{-4} T^2$  | J/kgK             |
| Viscosity              | $\ln \mu = \frac{556.835}{T} - 0.3958 \ln T - 6.4406$  | Pa-s              |
| Thermal conductivity   | $k = 110 - 0.0648T + 1.16 \times 10^{-5} T^2$  | W/mK              |

358

### 359 3.3 Model validation

360 The model for the nitrogen CBC was verified with results of numerical model reported by Ahn  
 361 and Lee [7]. The input parameters used for the validation are shown in Table 2. In Table 3, the  
 362 main results of the cycle model are compared with the literature values. The results of the cycle  
 363 model agreed well with the results obtained from literature to within 0.86%. The small  
 364 dissimilarities in the results could be due to the thermodynamic properties calculations and the  
 365 round-off error in the input parameters. Therefore, the developed Matlab cycle model is  
 366 deemed accurate enough for simulating the performance of the nitrogen CBC.

367 **Table 2**  
 368 Input parameters for the validation of the nitrogen CBC. Data taken from Ahn and Lee [7]

| Parameters                     | Value     |
|--------------------------------|-----------|
| Cycle maximum pressure         | 181.5 bar |
| LPC/HPC inlet temperature      | 27 °C     |
| Turbine inlet temperature      | 500 °C    |
| IHX Na side inlet temperature  | 526 °C    |
| IHX Na side outlet temperature | 450 °C    |
| Recuperator minimum TTD        | 14.2 °C   |
| Turbine efficiency             | 90%       |
| LPC/HPC efficiency             | 85%       |
| Thermal work                   | 150 MW    |

369

370

371

372

373

374

375 **Table 3**  
 376 Validation of cycle model against literature value

| Parameters                    | Literature value [7] | Simulation value | Relative difference (%) |
|-------------------------------|----------------------|------------------|-------------------------|
| Precooler inlet temperature   | 90.7 °C              | 90.6 °C          | 0.11                    |
| LPC outlet temperature        | 59.4 °C              | 59.4 °C          | 0                       |
| HPC outlet temperature        | 76.5 °C              | 76.5 °C          | 0                       |
| IHX N2 side inlet temperature | 348.7 °C             | 348.6 °C         | 0.03                    |
| Turbine outlet temperature    | 373.3 °C             | 373.4 °C         | 0.03                    |
| Recuperator effectiveness     | 95%                  | 95.1%            | 0.11                    |
| Nitrogen mass flow            | 2510.0 kg/s          | 2508.9 kg/s      | 0.04                    |
| Thermal efficiency            | 34.9%                | 35.2%            | 0.86                    |

377

### 378 3.4 Assumptions and settings

379 Some boundary conditions and parameters have to be set in order to evaluate the  
 380 thermodynamic performance of the cycles. In this study, the selection of the boundary  
 381 conditions and parameters were done within the limits allowed by the state-of-the-art in  
 382 component technologies (e.g. turbine and compressor) and values obtained in open literatures  
 383 [3, 7, 35, 44].

384 Therefore, the following assumptions and settings were used for the thermodynamic  
 385 performance calculation:

- 386 • Steady state full power rating conditions were assumed
- 387 • Negligible heat losses to the surrounding except through the cooling water in precooler  
 388 and intercooler
- 389 • The heat source was assumed to be a SM-SFR with a constant reactor thermal input  
 390 of 500 MW
- 391 • A reactor core outlet temperature of 545 °C and pressure of 1.15 bar were selected  
 392 while IHX Na side outlet temperature was set to 395 °C
- 393 • Since pipe design is outside the scope of this study, the pressure losses along the pipes  
 394 were set to zero
- 395 • Pressure loss through the reactor core was set at 3.74 bar
- 396 • Turbomachinery were assumed to be adiabatic with isentropic efficiencies of 93%,  
 397 89%, 88% and 82% for the turbines, LP compressors, HP compressors and pump  
 398 respectively
- 399 • LPC and HPC inlet temperatures were set at 27 °C
- 400 • Heat exchangers were designed as Printed Circuit Heat Exchanger (PCHE) type.
- 401 • Heat exchanger models were based on the TTD (or pinch) approach. Specifying heat  
 402 exchanger performance in term of minimum TTD or pinch, instead of effectiveness,  
 403 is considered to be a more realistic measure of what is achievable [45]
- 404 • Turbine inlet temperature was set to 530 °C. This has been selected higher than the  
 405 values reported in most literature since this study eliminates the use of intermediate  
 406 sodium loop
- 407 • Recuperator minimum TTD was set to 15 °C
- 408 • Precooler and intercooler cooling water inlet temperatures were assumed to be  
 409 available at 20 °C. Hence the precooler and intercooler TTD was about 7 °C
- 410 • Generator efficiency was taken to be 98.7%
- 411 • Maximum cycle pressure at HPC outlet was set at 180 bar

- 412       • The compressors inlet pressures were defined by the optimum pressure ratios, which  
413       were determined by optimisation to the cycle efficiency

414       These assumed baseline conditions and parameters only represent a realistic starting point for  
415       cycle performance calculation and comparison. Hence for sensitivity analysis, some of these  
416       values could be varied to examine their effects on the cycle performance and component  
417       design.

## 418       **4 Preliminary design of heat exchangers and** 419       **turbomachinery**

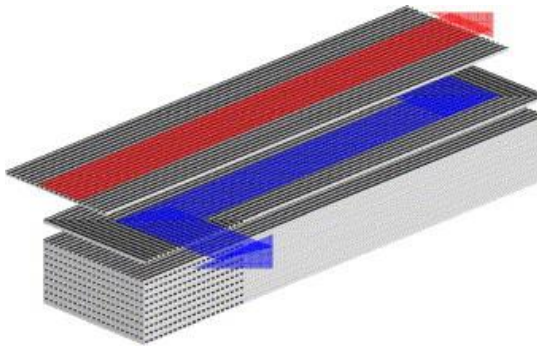
420       The main components having significant impact on the performance and size of CBC are the  
421       heat exchangers and turbomachinery. Therefore, this section describes the methodology for  
422       their preliminary design and sizing. Design of the primary circuit components such as the  
423       reactor and sodium pump was not considered. Also piping design was not examined.

### 424       **4.1 Heat exchanger design and sizing methodology**

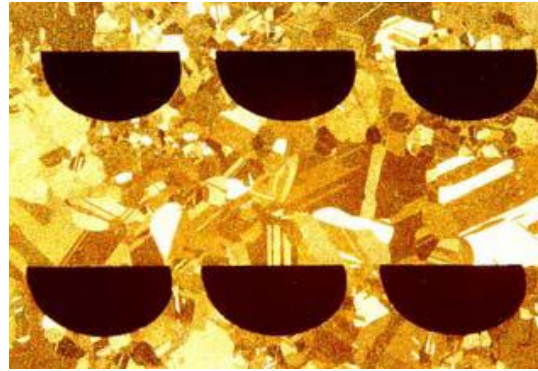
425       Preliminary design and sizing was done for the following heat exchangers: Na/N<sub>2</sub> IHX,  
426       recuperator, precooler and intercooler. Appropriate selection and design of heat exchangers  
427       for CBC is important because [46]: (1) The volume of the heat exchangers will largely  
428       determine the footprint of the CBC and hence the capital cost (2) The effectiveness and  
429       pressure losses through the heat exchangers will impact the cycle efficiency and hence the  
430       operating cost (3) Reliable heat exchangers that is able to withstand the CBC's high pressure  
431       and temperature will guarantee the safety of the plant.

432       All the heat exchangers in this work were assumed to be of the PCHE type. Most previous  
433       studies settled on the PCHE as the heat exchanger of choice for CBC [17, 44, 47] . This is due  
434       to its compactness, reliable mechanical characteristics at high pressure and temperature and  
435       the high effectiveness [48]. Heatric Ltd (UK) has been the sole manufacturer of PCHE since  
436       1985. PCHEs are constructed from flat metal plates into which fluid flow channels are photo-  
437       chemically etched into one side of the plate. The etched-out plates are then stacked and  
438       diffusion bonded together to form strong, compact, all-metal heat exchanger module as shown  
439       in Figure 4. The etched channels are usually semi-circular in cross-section with typical  
440       diameter of 1.0 – 5.0 mm and depth of 0.5 – 2.5 mm [49]. According to Heatric, it is possible  
441       to manufacture PCHE module with size up to 900 mm (width) by 900 mm (height) by 2500  
442       mm (length) if desired [35]. The calculations in this work were based on the standard plate  
443       and flow channel specifications shown in Table 4. The hot and cold plate specifications were  
444       assumed to be the same. Straight flow channels with counter-current flow arrangement was  
445       also assumed in the design. Depending on the required thermal duty, a number of identical  
446       modules are then welded together to form the complete heat exchanger unit [50].

447



a. PCHE plate stacking



b. Micrograph section through diffusion bonded core

448 *Figure 4 Printed circuit heat exchanger construction (courtesy of Heatric)*

449 **Table 4**  
450 Selected PCHE specifications

| Specification    | Value                |
|------------------|----------------------|
| Material         | 316L Stainless steel |
| Channel diameter | 1.5-2 mm             |
| Channel pitch    | 1.9 - 2.4 mm         |
| Plate thickness  | 1-1.5 mm             |
| Module width     | 900 mm               |
| Module height    | about 900 mm         |
| Module length    | <= 2500 mm           |

451

452 A preliminary heat exchanger design code, which can be integrated with the cycle calculation  
 453 code, was developed in Matlab. The cycle calculation provided some of the initial design  
 454 conditions such as the fluid types, mass flow rates, inlet and outlet enthalpies, inlet pressures  
 455 and effectiveness. The heat exchanger design code then uses the given initial design conditions,  
 456 the PCHE plate specifications and the desired maximum pressure drop to estimates the size  
 457 and mass of the heat exchanger. The code calculates the flow frontal cross section area (width  
 458 X height) and the length of the heat exchanger that meet the required effectiveness while  
 459 satisfying the maximum pressure loss requirement. The design was carried out based on the  
 460 logarithmic mean temperature difference (LMTD) method. For proper determination of fluid  
 461 properties within the heat exchanger, the flow paths along the heat exchanger is discretised  
 462 into N number of thermal nodes as shown in Figure 5. The specific heat of the fluid can be  
 463 assumed to be constant within the thermal nodes such that the LMTD can be calculated as  
 464 follows:

$$LMTD = \frac{(T_{ho} - T_{ci}) - (T_{hi} - T_{co})}{\ln \frac{(T_{ho} - T_{ci})}{(T_{hi} - T_{co})}} \quad (20)$$

465

466 The heat transferred is given by:

$$Q = \dot{m}_c(h_{co} - h_{ci}) = \dot{m}_h(h_{hi} - h_{ho}) = U \cdot A \cdot LMTD \quad (21)$$

467

468 The overall heat transfer coefficient, U was determined from the convective heat transfer  
 469 coefficients and conduction through the heat exchanger material as follows:

$$\frac{1}{U} = \frac{1}{h_h} + \frac{t}{k} + \frac{1}{h_c} \quad (22)$$

470 Where,

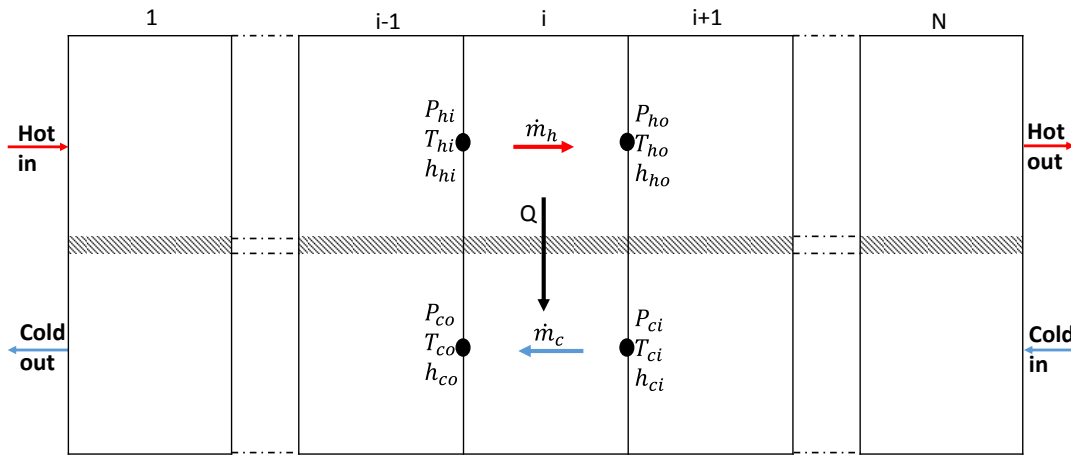
471  $h_h$  is the convective heat transfer coefficient on the hot side

472  $h_c$  is the convective heat transfer coefficient on the cold side

473 Convective heat transfer coefficients were determined based on the Nusselt number formula:

$$Nu = \frac{hD_h}{k} \quad (23)$$

474 Where  $D_h$  is the hydraulic diameter



475  
 476 *Figure 5 Nodalization of Heat exchanger*

477 For Nitrogen and water, the heat transfer behaviour was estimated by using the Hesselgraves'  
 478 recommendation for laminar flow and Gnielinski's correlation for turbulent flow as follows[51,  
 479 52]:

- 480 • Laminar flow ( $Re \leq 2300$ )

$$Nu = 4.089 \quad (24)$$

- 481 • Turbulent flow ( $Re \geq 5000$ )

$$Nu = \frac{\frac{f}{8}(Re - 1000)Pr}{1 + 12.7(Pr^{2/3} - 1)\sqrt{\frac{f}{8}}} \quad (25)$$

483  
 484 Where  $f$  is the friction factor that can be obtained from the Moody chart or the  
 485 Colebrook-White correlation:

$$\frac{1}{\sqrt{f}} = -2.0 \log \left( \frac{\epsilon/D_h}{3.7} + \frac{2.51}{Re\sqrt{f}} \right) \quad (26)$$

486

487 • Transition region ( $2300 < Re < 5000$ )

$$Nu = 4.089 + \frac{Nu_{Re=5000} - 4.089}{5000 - 2300} (Re - 2300) \quad (27)$$

488

489 For liquid sodium, the Nusselt number was calculated from the Lockart-Martinelli correlation:

$$Nu = 5.0 + 0.025(RePr)^{0.8} \quad (28)$$

490

491 Pressure loss,  $\Delta P$  inside the channel of length  $L$  and hydraulic diameter  $D_h$  is defined as:

$$\Delta P = f \frac{L}{D_h} \frac{\rho V^2}{2} \quad (29)$$

492

493 Where the Darcy friction factor,  $f$  for laminar flow is given by:

$$f = \frac{64}{Re} \quad (30)$$

494

495 For fully turbulent flow ( $Re > 4000$ ), the Darcy friction factor is given by the Colebrook-White  
496 correlation in equation (26).

497 The heat exchanger thermal-hydraulic design is an iterative process done to achieve the  
498 specified effectiveness (or thermal duty) while ensuring that the desired pressure loss was  
499 maintained. The total thermal duty is divided equally among the thermal nodes and uniform  
500 heat flux is assumed in each node. The calculation can start from either the cold end or the hot  
501 end with an initial guess of flow frontal area. Equation (20) to (30) are then applied to  
502 determine the fluid conditions, heat transfer coefficients, pressure losses and length of each  
503 node. Subsequently, the heat exchanger length and pressure losses on the hot and cold sides  
504 are calculated. The calculated pressure loss is compared to the desired pressure loss and if  
505 different, a new guess value for the frontal area is selected. The calculation process is repeated  
506 until the desired pressure loss is obtained. However, if the calculated length is more than the  
507 maximum permissible channel length (2500 mm in this case), a new desired pressure loss is  
508 set. Finally, the height, number of module, volume, surface area and mass of the heat  
509 exchanger are calculated.

## 510 4.2 Turbomachinery design and sizing methodology

511 The boundary conditions and component parameters selected for the thermodynamic cycles  
512 will influence the characteristics and size of the turbomachinery. Hence, preliminary design  
513 and sizing was done for the compressors and the turbines in order to highlight the effects of  
514 the cycle specifications on the turbomachinery, besides their impact on cycle efficiency. For  
515 the nitrogen cycles considered, all the turbomachinery were assumed to be of the axial type  
516 due to the large volume flow. Thermodynamic cycle calculation results and specifications such  
517 as shaft power or mass flow rate, inlet temperature and pressure, pressure ratio and isentropic  
518 efficiency will serve as input design requirements.

519 The similarity concept is a very common approach for conceptual/preliminary design of  
520 turbomachinery [28, 47, 53-56]. It is based on the selection of two dimensionless numbers,  
521 specific speed ( $n_s$ ) and specific diameter ( $d_s$ ), in conjunction with the use of Balje's  $n_s$ - $d_s$   
522 diagrams [57].  $n_s$  and  $d_s$  can be determined from equation (31) and equation (32):

$$n_s = \frac{\omega\sqrt{\dot{Q}}}{(gH_{ad})^{3/4}} \quad (31)$$

523

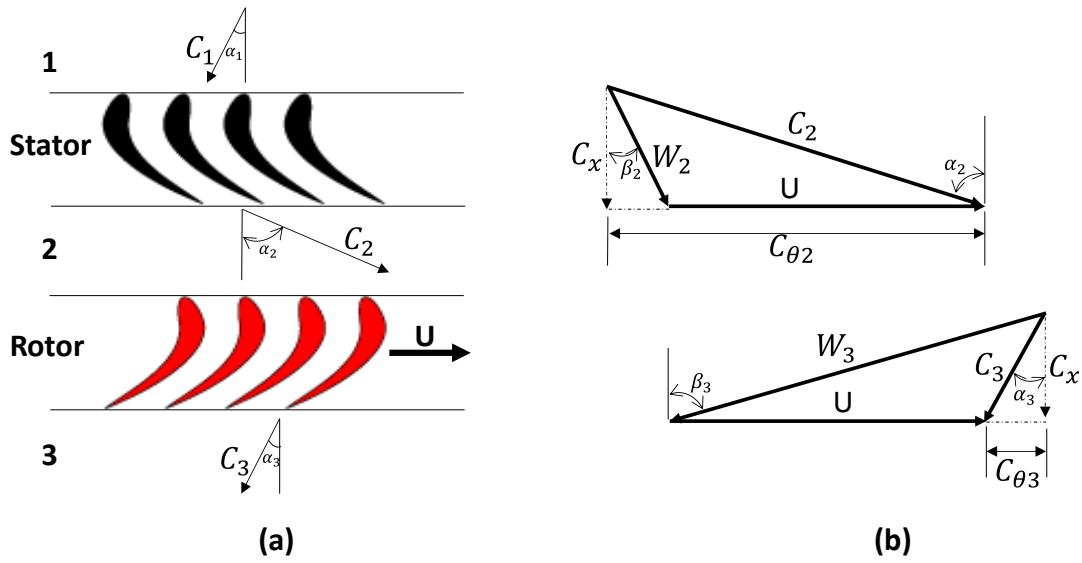
$$d_s = \frac{D(gH_{ad})^{1/4}}{\sqrt{\dot{Q}}} \quad (32)$$

524

525 Where  $\omega$  is shaft rotational speed,  $\dot{Q}$  is the volumetric flow rate,  $g$  is acceleration due to  
 526 gravity,  $H_{ad}$  is stage adiabatic head and  $D$  is the wheel diameter. From the  $n_s$ - $d_s$  diagrams, the  
 527 values of  $n_s$  and  $d_s$  needed to achieve the desired turbomachinery efficiency can be determined.  
 528 Since the volumetric flow rate and total adiabatic head are already fixed by the thermodynamic  
 529 cycle specifications, the only potential for optimising the turbomachinery design lies with the  
 530 choice of rotational speed and stage adiabatic head (or number of stages). For the grid  
 531 connected single shaft configuration, the rotational speed is also fixed and only the number of  
 532 stages is available for influencing the specific speed. Moreover, there is restriction on the  
 533 number of stages that can be utilized for turbomachinery design. On the contrary, the two shaft  
 534 configuration have the advantage to greatly influence the specific speed and hence optimise  
 535 the efficiency by changing the rotational speed of the compressor shaft.

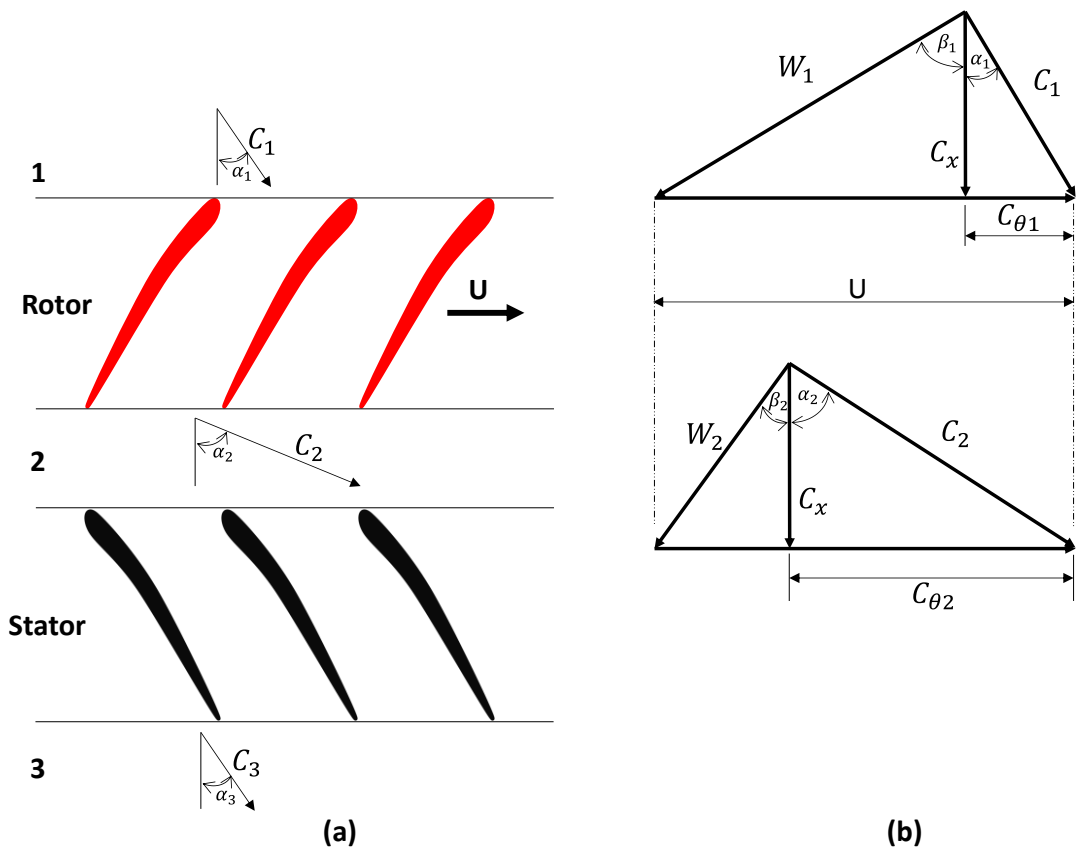
536 Even though the similarity concept provides a means to rapidly size the turbomachinery, the  
 537  $n_s$ - $d_s$  diagrams can only predict approximate value of efficiency. Also, it is only available for  
 538 single stage compressors and turbines. Therefore, in this study, a more exact but basic and  
 539 rational preliminary design methodology based on two-dimensional (2-D) mean-line approach  
 540 was employed. This is because it is not necessary at this initial stage to pursue a detailed design  
 541 of the turbomachinery. 2-D mean-line analysis means that the flow through the  
 542 turbomachinery is described by the magnitude and direction of gas velocity in the axial-  
 543 tangential coordinate at the mean blade height without considering any radial variation in gas  
 544 flow. Similarly, the thermodynamic properties of the working fluid were specified only at the  
 545 mean blade height. Thus, fast design solutions can be obtained at the initial phase of  
 546 turbomachinery design with the 2-D mean-line approach. It is considered a reasonable first  
 547 approximation for axial-flow turbomachinery with high hub-to-tip ratios greater than 0.8 [58,  
 548 59] .

549 The stator-rotor arrangements for axial-flow turbine and compressor are shown in Figure 6a  
 550 and Figure 7a respectively. Axial-flow turbine extracts energy from the working fluid by first  
 551 increasing the tangential velocity of the gas in a row of stator (or nozzle) blades then followed  
 552 by a row of rotor blades that convert the gas swirl into torque for the rotating shaft. On the  
 553 other hand, axial-flow compressor compresses the working fluid by first imparting kinetic  
 554 energy to the fluid by a row of rotor blades then followed by diffusion in a row of stator blades  
 555 to convert a part of the kinetic energy into static pressure. Several stages are usually needed in  
 556 axial-flow turbomachinery to attain the required pressure ratio. The relationship among the  
 557 velocities and flow angles at the inlet and outlet of the rotor is best illustrated with the velocity  
 558 diagrams at the mean blade height shown in Figure 6b and Figure 7b. The fluid enters the  
 559 turbine rotor row with a relative velocity,  $W_2$  at an angle,  $\beta_2$  and leaves with a relative  
 560 velocity,  $W_3$  at an angle,  $\beta_3$ . The rotor blade tangential velocity at the mean blade height is  $U$ .  
 561 Vectorial addition of the relative velocities and blade velocity yields the absolute velocities  $C_2$   
 562 and  $C_3$  at rotor inlet and outlet respectively. For the compressor, the fluid enters the rotor  
 563 with a relative velocity,  $W_1$  at an angle,  $\beta_1$  and leaves with a relative velocity,  $W_2$  at an angle,  $\beta_2$ .  
 564 The corresponding absolute velocities are  $C_1$  and  $C_2$  respectively.



565

566 *Figure 6 Axial turbine stator-rotor arrangement and velocity diagram*



567

568 *Figure 7 Axial compressor rotor-stator arrangement and velocity diagram*

569 Subscript x is used to represent the axial component of the gas velocities while subscript  $\theta$   
 570 represents the tangential components.

571 Turbomachinery design was performed with the following assumptions:

- 572 • The process through the rotor and stator is assumed to be adiabatic

- 573 • Constant mean-line blade radius,  $r_m$
- 574 • Constant axial-flow velocity,  $C_x$  throughout the turbomachinery stages
- 575 • Equal enthalpy changes per stage
- 576 • Repeating stages used except the first stage of the turbine and final stage of the
- 577 compressor

578 Euler turbomachinery equation governing the energy transfer in a turbine stage is given as:

$$\Delta h_0 = U(C_{\theta 2} + C_{\theta 3}) \quad (33)$$

579 For compressor stage, the Euler equation is given as:

$$\Delta h_0 = U(C_{\theta 2} - C_{\theta 1}) \quad (34)$$

580 Where,

581  $\Delta h_0$  is the difference in stagnation enthalpy between the stage inlet and exit

582  $C_{\theta 1}$  is the tangential component of absolute velocity at stage inlet

583  $C_{\theta 2}$  is the tangential component of absolute velocity at stator exit for turbine or rotor

584 exit for compressor

585  $C_{\theta 3}$  is the tangential component of absolute velocity at stage exit

586 The velocity diagrams can be defined by three parameters: flow coefficient, stage loading

587 coefficient and reaction.

588 The flow coefficient,  $\phi$  is defined as the ratio of axial flow velocity,  $C_x$  to the blade velocity,

589  $U$ :

$$\phi = \frac{C_x}{U} \quad (35)$$

590

591 The stage loading coefficient,  $\psi$  which is a measure of the work done in a stage is defined as:

$$\psi = \frac{\Delta h_0}{U^2} \quad (36)$$

592

593 Degree of reaction,  $\Lambda$  shows the fraction of the expansion or compression which occurs in the

594 rotor. It is defined as:

$$\Lambda = \frac{\Delta h_{rotor}}{\Delta h_{stage}} \quad (37)$$

595 Where,

596  $\Delta h_{rotor}$  is the difference in static enthalpy between rotor inlet and exit

597  $\Delta h_{stage}$  is the difference in static enthalpy between the stage inlet and exit

598 Turbine stage performance is specified by total-to-total stage isentropic efficiency and the

599 stator loss coefficient. Turbine stage isentropic efficiency is defined as the ratio of actual work

600 per unit mass to the ideal work per unit mass between the same total pressures:

$$\eta_{T,tt} = \frac{h_{01} - h_{03}}{h_{01} - h_{03,is}} \quad (38)$$

601 Where,

602  $\eta_{T,tt}$  is the turbine stage total-to-total isentropic efficiency

603  $h_{01}$  is the stagnation enthalpy at stage inlet

604  $h_{\theta 3}$  is the stagnation enthalpy at stage exit  
 605  $h_{03,is}$  is the ideal stagnation enthalpy at stage exit with isentropic expansion or  
 606 compression

607 The loss coefficient of turbine nozzle blade is determined by the Soderberg's correlation of  
 608 nominal loss coefficient,  $\xi$ :

$$\xi = 0.04 + 0.06 \left( \frac{\delta}{100} \right)^2 \quad (39)$$

609 Where  $\delta$  is the fluid deflection through the blade.

610 The loss coefficient is then defined in terms of kinetic energy from the nozzle blade row as  
 611 [60] :

$$h_2 - h_{2,is} = 1/2 C_2^2 \xi \quad (40)$$

612 Where,

613  $h_2$  is the static enthalpy at blade exit  
 614  $h_{2,is}$  is the ideal static enthalpy at blade exit with isentropic process  
 615  $C_2$  is the absolute velocity at blade exit

616 Compressor stage total-to-total efficiency,  $\eta_{C,tt}$  is defined as the ratio of the ideal work to the  
 617 actual work:

$$\eta_{C,tt} = \frac{h_{03,is} - h_{01}}{h_{03} - h_{01}} \quad (41)$$

618

619 Since the stage pressure ratios approach unity in this design, the stage efficiency was assumed  
 620 the same as the polytropic efficiency of the turbomachinery [61] .

621 The compressor blade loading is assessed by the Liebelin's diffusion factor and de Haller  
 622 number given in equation (42) and equation (43) respectively:

$$DF = 1 - \frac{V_o}{V_i} + \frac{\Delta V_{\theta}}{2\sigma V_i} \quad (42)$$

623

$$dHaller = \frac{V_o}{V_i} \quad (43)$$

624 Where,

625  $V_i$  and  $V_o$  are the blade inlet and outlet velocity respectively  
 626  $\Delta V_{\theta}$  is the change in tangential velocity  
 627  $\sigma$  is the blade solidity, which is the ratio of the blade chord to spacing (c/s)

628 To prevent excessive flow diffusion and potential separation, the diffusion factor should be  
 629 restricted to below 0.6 and/or the de Haller number should be kept above 0.72. The diffusion  
 630 factor is used to select the blade solidity which is then used together with the aspect ratio to  
 631 determine the blade numbers. Aspect ratio, AR is defined the ratio of blade height,  $b_H$  to blade  
 632 chord, c:

$$AR = \frac{b_H}{c} \quad (44)$$

633

634 For turbine, Zweifel's criterion for optimum lift coefficient,  $C_{L,op}$  is used to determine the  
635 solidity as follows:

$$C_{L,op} = \left| \frac{2}{\sigma_x} \cos^2 \alpha_o (\tan \alpha_i - \tan \alpha_o) \right| \quad (45)$$

636 Where,

637  $\sigma_x$  is solidity based on axial blade chord

638  $\alpha_i$  and  $\alpha_o$  are the flow angles at blade inlet and outlet respectively

639 A value of 0.8 is selected for the optimum lift coefficient.

640 Annulus flow area,  $A$  and blade height,  $b_H$  can be calculated with the help of mass continuity  
641 in equation (46) and equation (47).

$$\dot{m} = \rho A C_x \quad (46)$$

642

$$A = 2\pi r_m b_H \quad (47)$$

643 The mean radius,  $r_m$  is obtained from:

$$U = r_m \omega \quad (48)$$

644

645 The number of blade,  $N_b$  is determined from:

$$N_b = \frac{2\pi r_m}{s} \quad (49)$$

646

647 Two separate axial-flow turbomachinery design codes were developed in Matlab for the mean-  
648 line aerothermodynamic design of the compressors and turbines using the above equations.  
649 The design was able to estimate the turbomachinery flowpath geometry, blade heights, gas  
650 velocities and flow angles, stage number and volume based on the desired input design  
651 requirements obtained from cycle analysis. The main design variables included rotational  
652 speed, flow coefficient, stage number, mean blade velocity and inlet flow angle.  
653 Thermodynamic properties of the working fluid were obtained from NIST REFPROP property  
654 program. Static conditions of the fluid were calculated from the stagnation conditions based  
655 on the fundamental principle rather than ideal gas approximation. Similarly, calculations for  
656 expansion and compression processes were based on enthalpy instead of the use of constant  
657 or average specific heat capacity value. Hence, the codes can be applied to working fluid with  
658 real gas properties such as s-CO<sub>2</sub>. The turbomachinery design outcome can provide a basis for  
659 comparison among different cycles as well as highlighting the impact of various choices of  
660 design variables. Also in future work, the preliminary design code can be improved further  
661 with the capability for blade profile design, span-line design and generation of performance  
662 map for off-design analysis and dynamic modelling.

## 663 5 Results and discussion

664 CBC using nitrogen as working fluid and coupled to SM-SFR was investigated through two  
665 cycle configurations: a reference single shaft configuration and a two-shaft configuration with  
666 parallel turbines. This section presents the comparison of the two configuration in terms of  
667 thermodynamic performance and component design variables.

## 668 5.1 Thermodynamic performance

669 Results of the thermodynamic analysis at the baseline boundary conditions and cycle  
670 parameters for each of the two cycle configurations studied is the main output of this section.  
671 Hence this will form the basis of thermodynamic performance comparison between the two  
672 cycle configuration options.

673 The Matlab cycle analysis code was used to build a thermodynamic model of the CBCs  
674 coupled to SFR using the equations listed in Section 3. A summary of the baseline boundary  
675 conditions and parameters used to evaluate the thermodynamic performance of both the  
676 reference single-shaft configuration and the proposed two-shaft alternative is shown in Table  
677 5. The boundary conditions (or input variables) include reactor thermal power, reactor outlet  
678 temperature and pressure, Na/N<sub>2</sub> IHX primary side outlet temperature, turbine inlet  
679 temperature, HPC outlet pressure, LPC inlet pressure, LPC and HPC inlet temperature and  
680 cooling water temperature. Typical design parameters such as minimum TTD, heat exchanger  
681 and reactor pressure losses, turbomachinery isentropic efficiencies and generator efficiency  
682 were used. The input variables and cycle parameters were selected to be the same values for  
683 both the single-shaft configuration and the two-shaft alternative. This will ensure a reasonable  
684 comparison between the two cycles.

685 **Table 5**  
686 Boundary conditions and cycle parameters

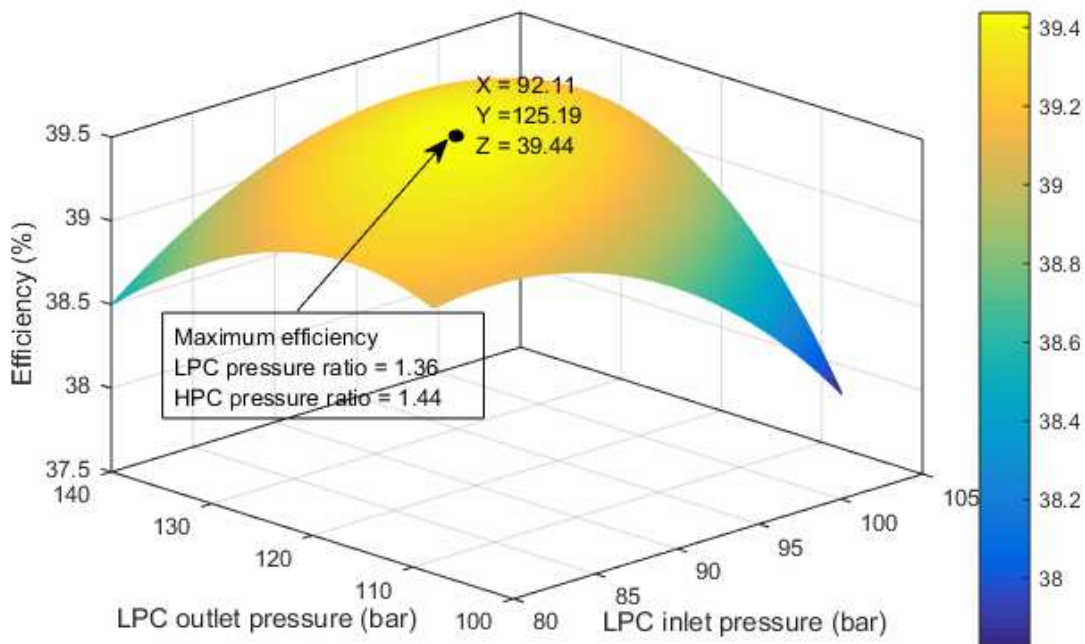
| Parameter/Variables                 | Value |
|-------------------------------------|-------|
| Reactor thermal power (MW)          | 500   |
| Core outlet temperature (°C)        | 545   |
| Core outlet pressure (bar)          | 1.15  |
| Core pressure loss (bar)            | 3.74  |
| IHX Na side outlet temperature (°C) | 395   |
| Turbine inlet temperature (°C)      | 530   |
| HPC outlet pressure (bar)           | 180   |
| LPC and HPC inlet temperatures (°C) | 27    |
| Cooling water temperature (°C)      | 20    |
| Recuperator TTD (°C)                | 15    |
| Turbomachinery efficiency (%):      |       |
| Turbines                            | 93    |
| LP compressor                       | 89    |
| HP compressor                       | 88    |
| Pump                                | 82    |
| Generator efficiency (%)            | 98.7  |

687

688 As far as possible, heat balance calculation should aim at achieving the maximum cycle  
689 efficiency. Only the compressors' pressure ratios are left as variables for optimising the cycle  
690 efficiency. Therefore, optimum pressure ratios of the LPC and HPC which make each cycle to  
691 reach the maximum thermal efficiencies were determined under the constraints of the specified  
692 input variables and cycle parameters. In Figure 8, the cycle efficiency as a function of the LPC  
693 inlet pressure and the LPC outlet is plotted. The cycle efficiency shows a maximum value at a  
694 LPC inlet pressure of 92.11 bar and a LPC outlet pressure of 125.19 bar (i.e. LPC pressure  
695 ratio of 1.36 and HPC pressure of 1.44 after taking into consideration the intercooler pressure  
696 loss). The optimum pressure ratios are the same for the two configurations. The Matlab code  
697 provides the mass flow rate, pressure, temperature and enthalpy of the working fluid at the  
698 inlet and outlet of all the cycle components. Also, the heat transferred and power produced or

699 absorbed in each component were calculated. Then the cycles' thermal efficiencies were  
700 calculated.

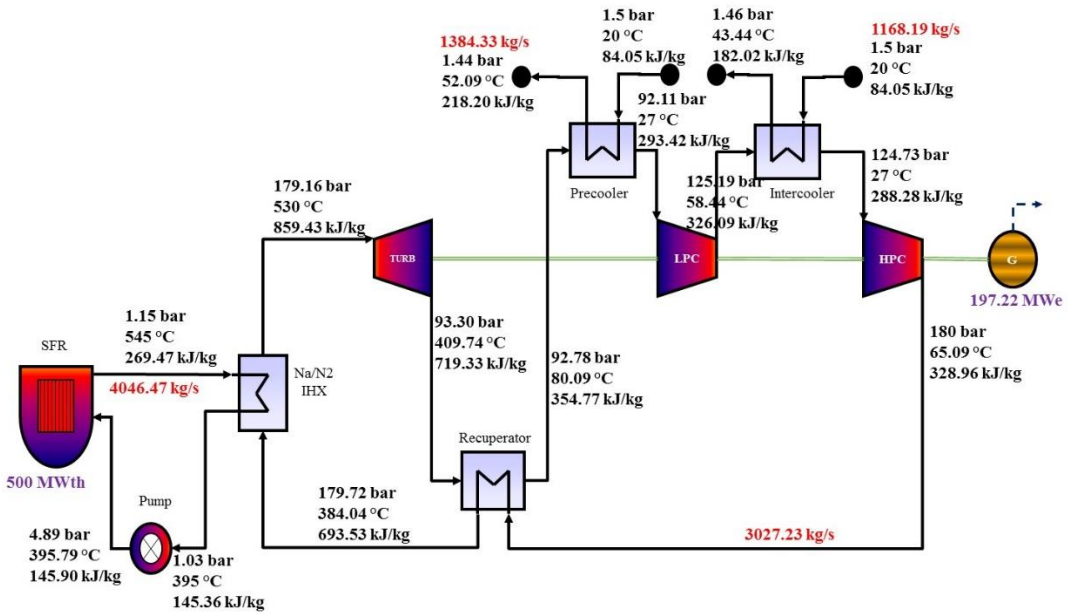
701 Remarkably, the proposed two shaft configuration is able to maintain the thermodynamic  
702 performance of the nitrogen cycle in addition to the potential for turbomachinery design  
703 optimisation with the free compressor shaft speed. It should be noted that previous studies  
704 indicated that two shaft configuration with series turbines usually leads to a deterioration of  
705 thermodynamic performance compared to single shaft configuration due to pressure loss in the  
706 connecting duct between the HP turbine and the LP turbine [40] . Figure 9 shows the  
707 thermodynamic state points of the reference single shaft intercooled configuration for the  
708 selected optimum conditions while Figure 10 shows those calculated for the proposed two  
709 shaft alternatives. Table 6 presents the major output variables of the thermodynamic  
710 performance analysis. The thermodynamic performance results indicated that the two  
711 configuration are similar in every respect except that the two shaft configuration employed  
712 two parallel turbines with the total flow divided between them.



713

714 *Figure 8 Cycle efficiency as a function of LPC inlet pressure and LPC outlet pressure for both configurations*

715



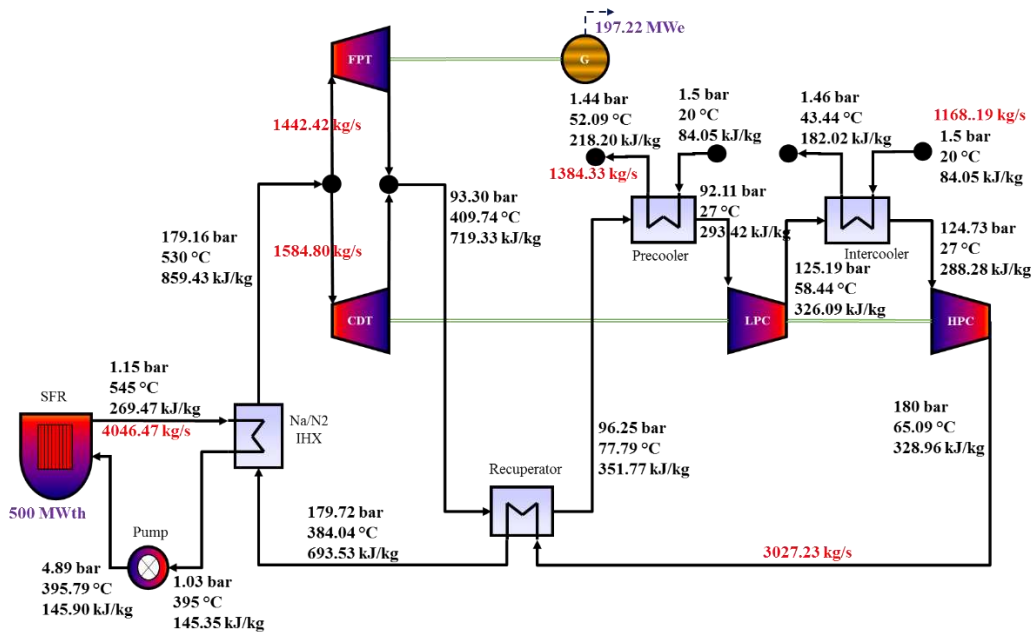
716

717 *Figure 9 Single shaft configuration thermodynamic state points*

718

719

720



721

722

723 *Figure 10 Two shaft configuration thermodynamic state points*

724

725

726 **Table 6**  
727 Thermodynamic performance result

| <b>Description</b>                  | <b>Single shaft</b> | <b>Two shaft</b> |
|-------------------------------------|---------------------|------------------|
| <b>Mass flow rates</b>              |                     |                  |
| Reactor mass flow                   | 4046.47 kg/s        | 4046.47 kg/s     |
| FPT                                 | -                   | 1442.42 kg/s     |
| CDT                                 | -                   | 1584.80 kg/s     |
| Total cycle mass flow               | 3027.23 kg/s        | 3027.23 kg/s     |
| Precooler cooling water             | 1384.33 kg/s        | 1384.33 kg/s     |
| Intercooler cooling water           | 1168.19 kg/s        | 1168.19 kg/s     |
| <b>Heat exchanger duty</b>          |                     |                  |
| Na/N <sub>2</sub> IHX               | 502.22 MW           | 502.22 MW        |
| Recuperator                         | 1103.63 MW          | 1103.63 MW       |
| Precooler                           | 185.70 MW           | 185.70 MW        |
| Intercooler                         | 114.45 MW           | 114.45 MW        |
| <b>Heat exchanger effectiveness</b> |                     |                  |
| Na/N <sub>2</sub> IHX               | 94.28 %             | 94.28 %          |
| Recuperator                         | 95.51 %             | 95.51 %          |
| Precooler                           | 88.06 %             | 88.06 %          |
| Intercooler                         | 81.41 %             | 81.41 %          |
| <b>Turbine power</b>                |                     |                  |
| CDT                                 | -                   | 222.02 MW        |
| FPT                                 | -                   | 202.07 MW        |
| Total turbine power                 | 424.09 MW           | 424.09 MW        |
| <b>Compressor power</b>             |                     |                  |
| LPC                                 | 98.88 MW            | 98.88 MW         |
| HPC                                 | 123.14 MW           | 123.14 MW        |
| Total compressor power              | 222.02 MW           | 222.02 MW        |
| <b>Pump load (MW)</b>               | 2.22 MW             | 2.22 MW          |
| <b>Pressure ratio (-)</b>           |                     |                  |
| LPC                                 | 1.36                | 1.36             |
| HPC                                 | 1.44                | 1.44             |
| Turbines                            | 1.92                | 1.92             |
| <b>Net electrical output</b>        | 197.22 MWe          | 197.22 MWe       |
| <b>Cycle efficiency</b>             | 39.44 %             | 39.44 %          |

728

## 729 5.2 Results of heat exchanger design

730 Heat exchangers of the nitrogen cycle include the Na/N<sub>2</sub> IHX, recuperator, precooler and  
731 intercooler. Input design conditions such as the inlet and outlet flow conditions, effectiveness  
732 and heat exchanger duties used for the preliminary sizing were obtained from the result of  
733 thermodynamic performance analysis given in Figure 9 or Figure 10, and Table 6. Since these  
734 values were the same for the single shaft and the two shaft configuration, the heat exchangers  
735 design will also be similar. The heat exchangers were discretised into ten thermal nodes. The  
736 results of the preliminary design calculations for the heat exchangers are given in Table 7. The  
737 temperatures of the heat exchangers' hot and cold streams at the inlet and outlet of the thermal  
738 nodes are shown in Figure 11.

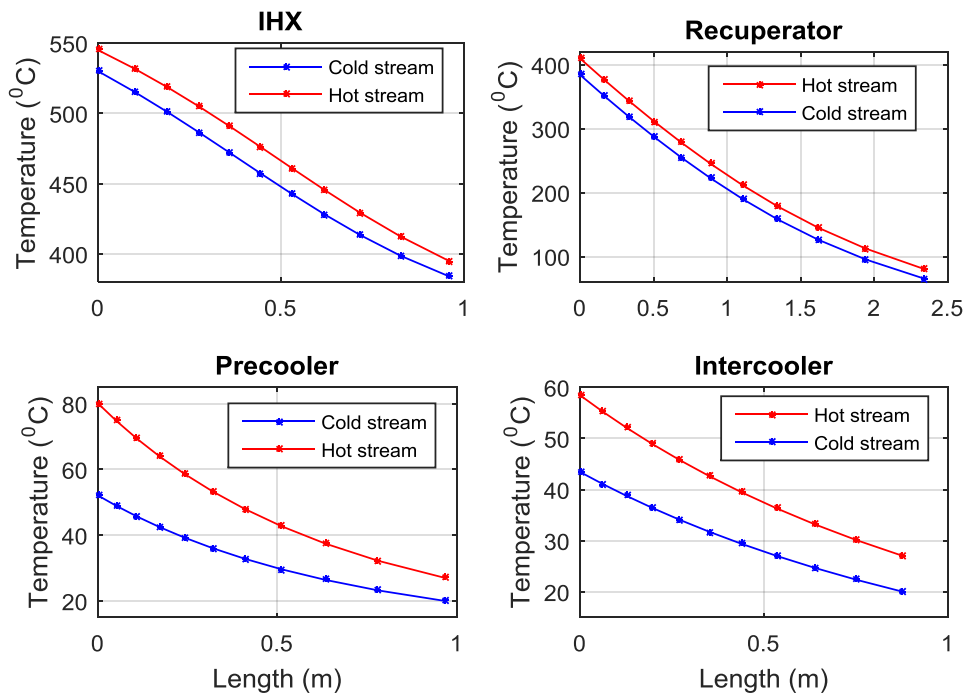
739 The volume of the recuperator alone constitute about 68% of the total volume of the heat  
740 exchangers, notwithstanding that the compactness of the recuperator has been improved by  
741 using smaller channel diameters, pitch and plate thickness. Any effort to reduce plant size and  
742 hence cost should therefore consider the selection and design of the recuperator. The relative

743 large volume of the recuperator is due to the large amount of recuperation and poor heat  
 744 transfer coefficient between nitrogen gas on both side of the recuperator compared with  
 745 sodium to nitrogen in the IHX or nitrogen to water in the pre-cooler and inter-cooler. Also, in  
 746 this study, conservative design approach was adopted with respect to the channel type, heat  
 747 conduction length and heat transfer correlation. Thus generally, the sizes of the heat  
 748 exchangers are likely to be reduced further with a different selection of channel type and a  
 749 more aggressive design assumption.

750 The 15 °C baseline minimum TTD chosen for the recuperator seems to be a good compromise  
 751 between the effect of TTD on recuperator volume and overall cycle efficiency. This is because  
 752 a slight increase in cycle efficiency by reducing the TTD below 15 °C comes at the cost of  
 753 very large increase in recuperator volume. The effects of changes in the TTD (or effectiveness)  
 754 of the recuperator on the overall cycle efficiency and volume of the recuperator are shown in  
 755 Figure 12. It can be seen that lower TTD causes higher cycle efficiency. A reduction of the  
 756 recuperator TTD from the baseline value of 15 °C to 5 °C results in a cycle efficiency increase  
 757 of about 3.3% point. However, the TTD has a significant effect on the volume and hence cost  
 758 of the recuperator. Decreasing the TTD has a non-linear effect on the recuperator size. The  
 759 same reduction of TTD from 15 °C to 5 °C results in a recuperator volume increase of about  
 760 986% point above the baseline value. On the other hand, an increase in TTD from 15 °C to  
 761 25 °C results in about 62% point reduction in recuperator size.

762 **Table 7**  
 763 Design parameters of heat exchangers

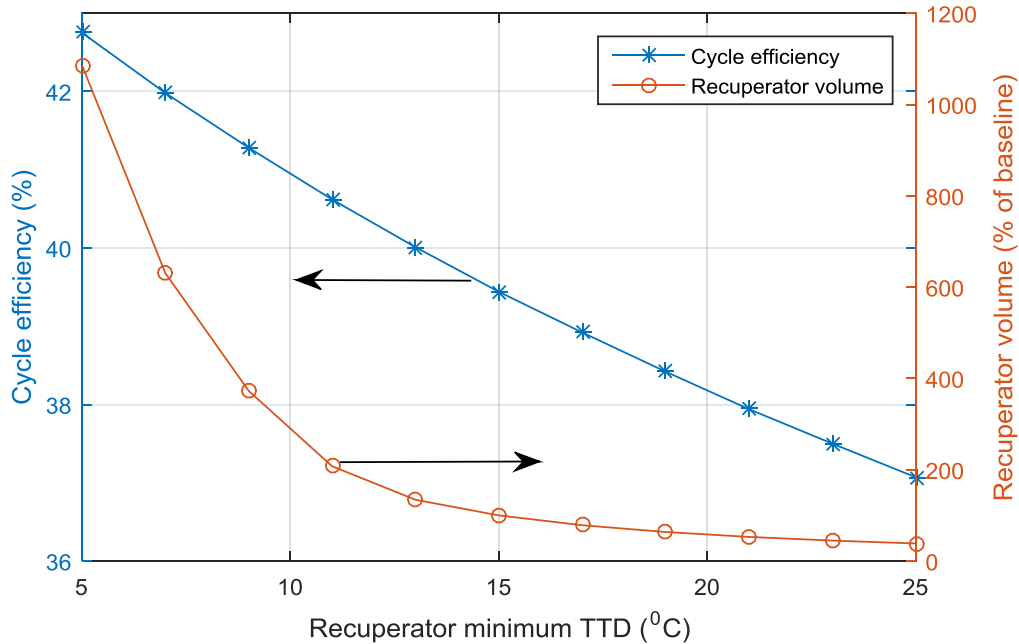
| <b>Description</b>                                     | <b>IHX</b>        | <b>Recuperator</b>             | <b>Pre-cooler</b>     | <b>Inter-cooler</b>   |
|--|-------------------|--------------------------------|-----------------------|-----------------------|
| Heat transfer duty (MW)                                | 502.22            | 1103.63                        | 185.70                | 114.45                |
| Fluid, hot side/cold side                              | Na/N <sub>2</sub> | N <sub>2</sub> /N <sub>2</sub> | N <sub>2</sub> /Water | N <sub>2</sub> /Water |
| Channel diameter (mm)                                  | 2                 | 1.5                            | 2                     | 2                     |
| Channel pitch (mm)                                     | 2.4               | 1.9                            | 2.4                   | 2.4                   |
| Plate thickness (mm)                                   | 1.5               | 1                              | 1.5                   | 1.5                   |
| Number of modules                                      | 29                | 63                             | 23                    | 23                    |
| Module width (mm)                                      | 900               | 900                            | 900                   | 900                   |
| Module height (mm)                                     | 883.56            | 894.04                         | 885.42                | 885.05                |
| Module length (mm)                                     | 959               | 2341.9                         | 967.3                 | 878.4                 |
| Free flow area (m <sup>2</sup> )                       | 5.03              | 11.79                          | 4                     | 4                     |
| Surface area density (m <sup>2</sup> /m <sup>3</sup> ) | 714.11            | 1014.8                         | 714.11                | 714.11                |
| Thermal density (MW/m <sup>3</sup> )                   | 22.70             | 9.30                           | 10.47                 | 7.11                  |
| Hot side pressure loss (kPa)                           | 12                | 52                             | 67                    | 46                    |
| Cold side pressure loss (kPa)                          | 56                | 28                             | 6                     | 4                     |
| Total core volume (m <sup>3</sup> )                    | 22.12             | 118.72                         | 17.73                 | 16.09                 |
| Total core mass (kg)                                   | 99736             | 508080                         | 79954                 | 72574                 |



765

766

Figure 11 Fluid temperature along heat exchanger length (all counter-current flow)



767

768

Figure 12 Effects of recuperator TTD on overall cycle efficiency and recuperator volume

### 769 5.3 Results of turbomachinery design

770

771

772

773

774

In this section, the result of the preliminary design and sizing of the turbomachinery based on 2-D meanline design is presented. The result gives the stage numbers and annular gas flow path geometry of the turbomachinery for the specified input design condition. This provides the basis for assessing the turbomachinery's contribution to the physical size of the plant as well as comparison between the single shaft and the proposed two shaft configuration. Table

775 8, Table 9 and Table 10 summarise and compare the respective design parameters for the  
776 turbines, the LPCs and the HPCs. These tables provide the number of stages, dimensionless  
777 design parameters, blade lengths, maximum diameters and other main features for all the  
778 turbomachinery.

779 The approach taken in this work was to design for approximately the same dimensionless  
780 parameters of flow coefficient, loading coefficient and reaction for the turbomachinery of the  
781 single shaft and two shaft configuration while maintaining the hub-to-tip ratio within  
782 acceptable limit. The target flow coefficient, stage loading coefficient and stage reaction for  
783 the turbines are about 0.6, 1.1 and 0.5 respectively while the respective values for the  
784 compressors are about 0.5, 0.3 and 0.55. The turbine dimensionless parameters were selected  
785 to be consistent with operation in the 93% efficiency and 60° nozzle outlet angle region of the  
786  $\phi$ - $\psi$  turbine plot. The  $\phi$ - $\psi$  plot was obtained from Saravanamuttoo et al. [62]. In the case of  
787 compressor, no such plot was found. Hence design data from literature was used as a guide in  
788 selecting the compressors' dimensionless parameters [63]. Low hub-to-tip ratio will increase  
789 secondary losses while too high hub-to-tip ratio will increase the impact of tip clearance losses.  
790 Therefore, as much as possible, the hub-to-tip ratio should be kept between 0.75 and 0.90. For  
791 the compressors, a de Haller number greater than 0.72 and a diffusion factor lower than 0.4  
792 are sought.

793 The main reasons for proposing two shaft configuration was to simplify the design of  
794 turbomachinery, to reduce turbomachinery size and to provide opportunity for improving cycle  
795 efficiency by increasing the efficiency of the turbomachinery.

### 796 **5.3.1 Turbomachinery design simplification**

797 A shaft speed of 8000 rpm was established as the optimum compressors/CDT rotational speed  
798 for the proposed two shaft configuration. The LPC, the HPC and the CDT of the two shaft  
799 layout can be freely designed since there is no requirement for a fixed rotational speed. For  
800 the reference single shaft configuration, the rotation speed was set to synchronise with the  
801 generator speed of 3000 rpm for grid frequency of 50 Hz. Therefore, its turbomachinery all  
802 rotate at this speed. Also for the proposed two shaft configuration, the rotational speed of the  
803 FPT is fixed at 3000 rpm. The fixing of the generator drive shafts at the synchronous speed  
804 will eliminate further losses from the use of gearbox to reduce shaft speed to 3000 rpm or  
805 electrical frequency converters to supply electric power at the grid frequency of 50 Hz.

806 The FPT was designed with one more stage numbers than the stages of the single shaft turbine  
807 in order to avoid a hub-to-tip ratio greater than the maximum limit. At a given rotational speed,  
808 the number of stages is proportional to the pressure ratio. Thus, the FPT and the single shaft  
809 turbine would normally be expected to have the same number of stages since they have the  
810 same pressure ratio and rotational speed. However, the hub-to-tip ratio and annular flow area  
811 are determined by the flow rate and axial velocity (or blade speed). The FPT's flow rate is  
812 lower than the single shaft turbine's flow rate. Therefore, FPT blade speed was reduced to  
813 keep the hub-to-tip ratio within acceptable limit while the stage number was increased to bring  
814 the loading coefficient to the target value.

### 815 **5.3.2 Size reduction of the turbomachinery**

816 Design calculation indicated that the total turbine volume is reduced from 3.24 m<sup>3</sup> in the single  
817 shaft configuration to 2.2 m<sup>3</sup> in the two shaft configuration due to the reduced tip diameters,  
818 although the total number of turbines stages is more for the two-shaft configuration. The size  
819 of turbomachinery is a function of both the stage numbers and the tip diameters. For the two  
820 shaft CDT, the rotational speed offers extra degree of freedom for design. Hence, the number  
821 of stages was reduced to one while appropriate selection of rotational speed was used to  
822 maintain the hub-to-tip ratio within the limits. Also, the high rotational speed of the CDT and

823 the reduced blade speed of the FPT lead to reduced tip diameters of the two-shaft configuration  
824 turbines compared to the single-shaft turbine.

825 For the compressors, the total compressors volume is reduced from 1.16 m<sup>3</sup> in the single shaft  
826 configuration to 0.2 m<sup>3</sup> in the two shaft configuration. The high rotational speed of the  
827 proposed two-shaft configuration resulted in reduced number of compressor stages and  
828 reduced tip diameters. In addition, the stage loading coefficient of the two shaft HPC is reduced  
829 further in order to keep the hub-to-tip ratio above the minimum limit.

### 830 5.3.3 Efficiency improvement

831 Favourable conditions exist in the proposed two shaft Brayton cycle for improving the  
832 turbomachinery efficiencies of the compressors and the CDT. The isentropic efficiencies of  
833 the LPC, the HPC and the turbines were assumed in the cycle calculation as 89%, 88% and  
834 93% respectively. These values were also used for the design of the turbomachinery. However,  
835 increasing the number of stages and changing the rotational speed are two methods for  
836 improving turbomachinery efficiency in a fixed cycle layout [7]. Therefore, the LPC, the HPC  
837 and the CDT of the two shaft cycle can be redesigned for a higher efficiency by increasing the  
838 number of stages and/or by changing the rotational speed. Better turbomachinery efficiencies  
839 will further improve the cycle performance. The effects of isentropic efficiencies of the LPC,  
840 the HPC and the CDT on the overall cycle efficiency are shown in Figure 13. The two shaft  
841 Brayton cycle shows about 0.29% point rise in cycle efficiency for each 1% point rise in CDT  
842 efficiency, about 0.22% point rise in cycle efficiency for each 1% point rise in LPC efficiency,  
843 and about 0.27% point rise in cycle efficiency for each 1% rise in HPC efficiency.

844

845

846 **Table 8**

847 Turbines design parameters and main features for the nitrogen cycles

| Parameters   | Single shaft | Two shaft |           |
|--|--------------|-----------|-----------|
|  |              | CDT       | FPT       |
| Number of stages in turbine                          | 3            | 1         | 4         |
| Flow coefficient                                     | 0.6          | 0.6       | 0.6       |
| Stage loading coefficient                            | 1.08         | 1.08      | 1.13      |
| Reaction   | 0.50         | 0.50      | 0.53      |
| Rotational speed, rpm                                | 3000         | 8000      | 3000      |
| Maximum tip diameter, mm                             | 1460         | 926       | 1210      |
| Maximum tip speed, m/s                               | 229          | 388       | 190       |
| Blade height, mm (min/max)                           | 85/135       | 41/66     | 56/89     |
| Hub/Tip ratio (min/max)                              | 0.81/0.88    | 0.86/0.90 | 0.85/0.90 |
| Blade numbers, (1 <sup>st</sup> stage stator/rotor)  | 20/76        | 25/79     | 26/103    |
| Blade chord, mm (1 <sup>st</sup> stage stator/rotor) | 264/284      | 139/177   | 173/260   |
| Axial length, mm                                     | 2007         | 304       | 1785      |
| Volume, m <sup>3</sup>                               | 3.24         | 0.2       | 2.0       |
| Aspect ratio   | 3            | 3         | 3         |
| Solidity   | 1.25         | 1.25      | 1.25      |
| Pressure ratio (-)                                   | 1.92         | 1.92      | 1.92      |
| Stage efficiency, %                                  | 92.60        | 93        | 92.55     |

848

849

850 **Table 9**  
 851 LPCs design parameters and main features for the nitrogen cycles.

| <b>Parameters</b>                                    | <b>Single shaft</b> | <b>Two shaft</b> |
|--|---------------------|------------------|
| Number of stages in LPC                              | 3                   | 1                |
| Flow coefficient                                     | 0.5                 | 0.5              |
| Stage loading coefficient                            | 0.29                | 0.29             |
| Reaction   | 0.55                | 0.55             |
| Rotational speed, rpm                                | 3000                | 8000             |
| Maximum tip diameter, mm                             | 1315                | 880              |
| Maximum tip speed, m/s                               | 207                 | 369              |
| Blade height, mm (min/max)                           | 67/82               | 63/79            |
| Hub/Tip ratio (min/max)                              | 0.88/0.90           | 0.82/0.85        |
| Blade numbers, (1 <sup>st</sup> stage rotor/stator)  | 64/66               | 45/50            |
| Blade chord, mm (1 <sup>st</sup> stage rotor/stator) | 73/71               | 68/61            |
| Axial length, mm                                     | 440                 | 140              |
| Volume, m <sup>3</sup>                               | 0.59                | 0.08             |
| Aspect ratio   | 1.1                 | 1.1              |
| Solidity   | 1.21                | 1.21             |
| Pressure ratio (-)                                   | 1.36                | 1.36             |
| Stage efficiency, %                                  | 89.32               | 89               |
| de Haller number                                     | 0.75                | 0.75             |
| Diffusion factor                                     | 0.39                | 0.38             |

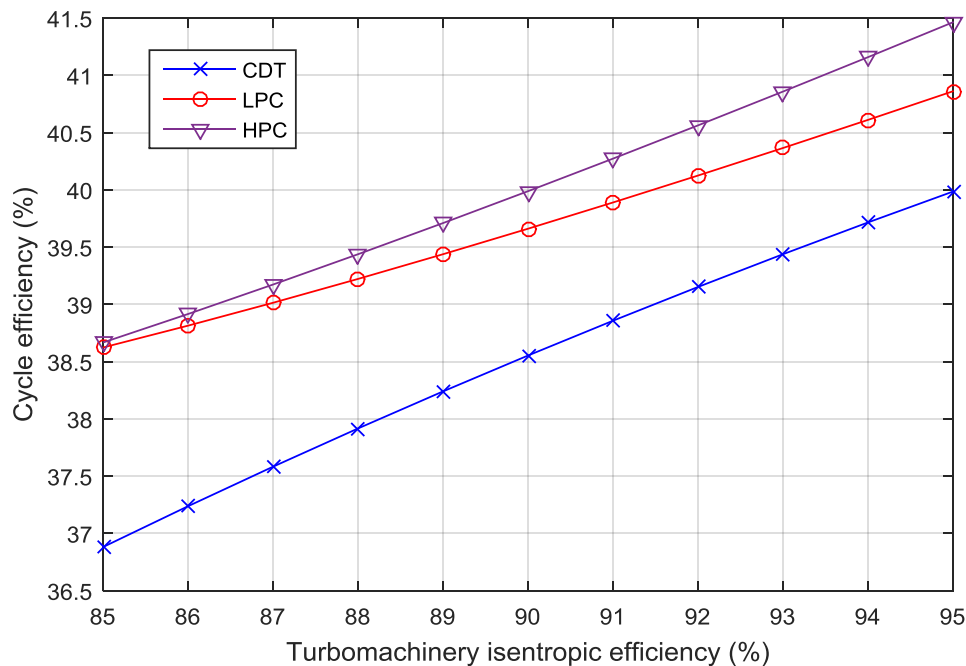
852

853

854 **Table 10**  
 855 HPCs design parameters and main features for the nitrogen cycles

| <b>Parameters</b>                                    | <b>Single shaft</b> | <b>Two shaft</b> |
|--|---------------------|------------------|
| Number of stages in HPC                              | 4                   | 2                |
| Flow coefficient                                     | 0.5                 | 0.5              |
| Stage loading coefficient                            | 0.29                | 0.25             |
| Reaction   | 0.55                | 0.55             |
| Rotational speed, rpm                                | 3000                | 8000             |
| Maximum tip diameter, mm                             | 1257                | 760              |
| Maximum tip speed, m/s                               | 197                 | 318              |
| Blade height, mm (min/max)                           | 65/52               | 62/79            |
| Hub/Tip ratio (min/max)                              | 0.90/0.92           | 0.79/0.83        |
| Blade numbers, (1 <sup>st</sup> stage rotor/stator)  | 77/80               | 37/39            |
| Blade chord, mm (1 <sup>st</sup> stage rotor/stator) | 58/48               | 70/66            |
| Axial length, mm                                     | 461                 | 279              |
| Volume, m <sup>3</sup>                               | 0.57                | 0.12             |
| Aspect ratio   | 1.1                 | 1.1              |
| Solidity   | 1.21                | 1.21             |
| Pressure ratio (-)                                   | 1.44                | 1.44             |
| Stage efficiency, %                                  | 88.46               | 88.31            |
| de Haller number                                     | 0.75                | 0.78             |
| Diffusion factor                                     | 0.39                | 0.34             |

856



857

858 *Figure 13 Effect of turbomachinery efficiencies on overall cycle efficiency*

## 859 **6 Conclusions**

860 In this study, thermodynamic analysis and preliminary design of nitrogen CBCs coupled to a  
 861 500 MWth SM-SFR have been presented. A reference single-shaft configuration and a  
 862 proposed two- shaft configuration with parallel turbines were investigated. Thermodynamic  
 863 performance assessment of the cycles, preliminary sizing of the heat exchangers and 2-D  
 864 mean-line aerodynamic design of the turbomachinery were performed using models developed  
 865 in Matlab.

866 As an outcome of this investigation the following main conclusions can be highlighted:

- 867 • Thermodynamic analysis of the cycles indicates that the proposed two shaft  
 868 configuration with parallel turbines have the same cycle thermodynamic efficiency of  
 869 39.44% as the reference single shaft configuration. In contrast, two shaft configuration  
 870 with turbines in series is known to result in loss of cycle efficiency.
- 871 • Heat exchangers preliminary sizing shows that the recuperator constitute a major  
 872 percentage of the total size. Therefore, any further effort to reduce the plant footprint  
 873 should focus on the selection and design of the recuperator.
- 874 • As expected, cycle efficiency decreases almost linearly with increase in the minimum  
 875 TTD of the recuperator while recuperator size decreases non-linearly with increase in  
 876 TTD. Hence, any reduction in volume obtained by increasing the TTD will be at the  
 877 cost of reduced cycle efficiency. A TTD of 15 °C appears to be a good compromise  
 878 between cycle efficiency and recuperator size.
- 879 • Preliminary design of the turbomachinery seems to reveal that the proposed two shaft  
 880 configuration could favour simplification of the design and reduced size as well as  
 881 increased cycle efficiency by improving the turbomachinery efficiency. The design of  
 882 the LPC, the HPC and the CDT of the two shaft configuration can be optimised with  
 883 the shaft rotational speed. An optimum compressors shaft speed of 8000 rpm is  
 884 established. Total compressors volume is reduced from 1.16 m<sup>3</sup> in the single shaft

885 configuration to 0.2 m<sup>3</sup> in the two shaft configuration while total turbine volume is  
886 reduced from 3.24 m<sup>3</sup> to 2.2 m<sup>3</sup>.

887 In the light of these findings, the proposed two-shaft CBC with nitrogen as working fluid could  
888 be a promising PCS for near-term demonstration of electricity generation from SFR. The  
889 current preliminary study neglected the impact of the pressure losses in the connecting pipes  
890 on the thermodynamic performance. Also the sizing of the heat exchangers is limited to the  
891 core, the sizes of the headers are not included. All these can be delayed till the detailed design  
892 phase. Nevertheless, this study provides considerable insight into the thermodynamic  
893 performance and preliminary sizing of heat exchangers and turbomachinery for nitrogen CBC  
894 coupled to SM-SFR.

895 Future studies should investigate opportunities for improving the heat transfer performance of  
896 the recuperator and hence reduction in recuperator size by (1) using wavy channel instead of  
897 straight channel type (2) assuming a shorter heat conduction length and (3) using a more  
898 radical heat transfer relationship obtained from experimental validation. On the other hand,  
899 more compact heat exchanger type such as the plate fin heat exchanger [64] should be  
900 investigated as substitute for the PCHE. However, this could be at the expense of the reduced  
901 risk of development offered by PCHE.

902

## 903 **Acknowledgement**

904 The authors would like to acknowledge GE Power (formerly ALSTOM Power Ltd) for  
905 financial support of this research.

## 906 **References**

- 907 [1] L. Damiani, A. P. Prato, and R. Revetria, "Innovative steam generation system for the  
908 secondary loop of "ALFRED" lead-cooled fast reactor demonstrator," *Applied Energy*,  
909 vol. 121, pp. 207-218, 2014.
- 910 [2] F. Carre, P. Yvon, P. Anzieu, N. Chauvin, and J.-Y. Malo, "Update of the French  
911 R&D strategy on gas-cooled reactors," *Nuclear Engineering and Design*, vol.  
912 240, no. 10, pp. 2401-2408, 2010.
- 913 [3] G. D. Pérez-Pichel, J. I. Linares, L. E. Herranz, and B. Y. Moratilla, "Thermal analysis  
914 of supercritical CO<sub>2</sub> power cycles: Assessment of their suitability to the forthcoming  
915 sodium fast reactors," *Nuclear Engineering and Design*, vol. 250, pp. 23-34, 2012.
- 916 [4] B. Merk, A. Stanculescu, P. Chellapandi, and R. Hill, "Progress in reliability of fast  
917 reactor operation and new trends to increased inherent safety," *Applied Energy*, vol.  
918 147, pp. 104-116, 2015.
- 919 [5] Gen IV International Forum (GIF), "Technology roadmap update for Generation IV  
920 nuclear energy systems," Nuclear Energy Agency (NEA) of the Organisation for  
921 Economic Co-operation and Development (OECD), Paris, 2014, Available:  
922 <https://www.gen-4.org/gif/upload/docs/application/pdf/2014-03/gif-tru2014.pdf>,  
923 Accessed on: 6 May 2015.
- 924 [6] P. G. Rousseau and J. P. Van Ravenswaay, "Thermal-fluid comparison of three-and  
925 single-shaft closed loop brayton cycle configurations for HTGR power conversion,"  
926 in *Proceedings of international congress on advances in nuclear power plants*  
927 *(ICAPP'03)*, Cordoba, Spain, 2003.
- 928 [7] Y. Ahn and J. I. Lee, "Study of various Brayton cycle designs for small modular  
929 sodium-cooled fast reactor," *Nuclear Engineering and Design*, vol. 276, pp. 128-141,  
930 2014.

- 931 [8] S. Hong, C. J. A. Bradshaw, and B. W. Brook, "Global zero-carbon energy pathways  
932 using viable mixes of nuclear and renewables," *Applied Energy*, vol. 143, pp. 451-459,  
933 2015.
- 934 [9] P. Eser, A. Singh, N. Chokani, and R. S. Abhari, "Effect of increased renewables  
935 generation on operation of thermal power plants," *Applied Energy*, vol. 164, pp. 723-  
936 732, 2016.
- 937 [10] A. S. Brouwer, M. van den Broek, W. Zappa, W. C. Turkenburg, and A. Faaij, "Least-  
938 cost options for integrating intermittent renewables in low-carbon power systems,"  
939 *Applied Energy*, vol. 161, pp. 48-74, 2016.
- 940 [11] V. Krakowski, E. Assoumou, V. Mazauric, and N. Maïzi, "Reprint of Feasible path  
941 toward 40–100% renewable energy shares for power supply in France by 2050: A  
942 prospective analysis," *Applied Energy*, vol. 184, pp. 1529-1550, 2016.
- 943 [12] G. D. Pérez-Pichel, J. I. Linares, L. E. Herranz, and B. Y. Moratilla, "Potential  
944 application of Rankine and He-Brayton cycles to sodium fast reactors," *Nuclear  
945 Engineering and Design*, vol. 241, no. 8, pp. 2643-2652, 2011.
- 946 [13] S. B. Seo, H. Seo, and I. C. Bang, "Adoption of nitrogen power conversion system for  
947 small scale ultra-long cycle fast reactor eliminating intermediate sodium loop," *Annals  
948 of Nuclear Energy*, vol. 87, Part 2, pp. 621-629, 2016.
- 949 [14] O. Olumayegun, M. Wang, and G. Kelsall, "Closed-cycle gas turbine for power  
950 generation: A state-of-the-art review," *Fuel*, vol. 180, pp. 694-717, 2016.
- 951 [15] J. R. Hoffmann and E. G. Feher, "150 kwe supercritical closed cycle system," *Journal  
952 of Engineering for Gas Turbines and Power*, vol. 93, no. 1, pp. 70-80, 1971.
- 953 [16] Y. Ahn *et al.*, "Review of supercritical CO<sub>2</sub> power cycle technology and current status  
954 of research and development," *Nuclear Engineering and Technology*, vol. 47, no. 6,  
955 pp. 647-661, 2015.
- 956 [17] V. Dostal, "A supercritical carbon dioxide cycle for next generation nuclear reactors,"  
957 PhD Thesis, Massachusetts Institute of Technology (MIT), Cambridge, Massachusetts,  
958 USA, 2004.
- 959 [18] L. Santini, C. Accornero, and A. Cioncolini, "On the adoption of carbon dioxide  
960 thermodynamic cycles for nuclear power conversion: A case study applied to  
961 Mochovce 3 Nuclear Power Plant," *Applied Energy*, vol. 181, pp. 446-463, 2016.
- 962 [19] X. Wang and Y. Dai, "Exergoeconomic analysis of utilizing the transcritical CO<sub>2</sub>  
963 cycle and the ORC for a recompression supercritical CO<sub>2</sub> cycle waste heat recovery:  
964 A comparative study," *Applied Energy*, vol. 170, pp. 193-207, 2016.
- 965 [20] R. V. Padilla, Y. C. Soo Too, R. Benito, and W. Stein, "Exergetic analysis of  
966 supercritical CO<sub>2</sub> Brayton cycles integrated with solar central receivers," *Applied  
967 Energy*, vol. 148, pp. 348-365, 2015.
- 968 [21] R. V. Padilla, Y. C. S. Too, R. Benito, R. McNaughton, and W. Stein,  
969 "Thermodynamic feasibility of alternative supercritical CO<sub>2</sub> Brayton cycles  
970 integrated with an ejector," *Applied Energy*, vol. 169, pp. 49-62, 2016.
- 971 [22] B. D. Iverson, T. M. Conboy, J. J. Pasch, and A. M. Kruiženga, "Supercritical CO<sub>2</sub>  
972 Brayton cycles for solar-thermal energy," *Applied Energy*, vol. 111, no. 0, pp. 957-  
973 970, 2013.
- 974 [23] S. J. Bae, Y. Ahn, J. Lee, and J. I. Lee, "Various supercritical carbon dioxide cycle  
975 layouts study for molten carbonate fuel cell application," *Journal of Power Sources*,  
976 vol. 270, pp. 608-618, 2014.
- 977 [24] M. Mecheri and Y. Le Moullec, "Supercritical CO<sub>2</sub> Brayton cycles for coal-fired  
978 power plants," *Energy*, vol. 103, pp. 758-771, 2016.
- 979 [25] S. Banik, S. Ray, and S. De, "Thermodynamic modelling of a recompression CO<sub>2</sub>  
980 power cycle for low temperature waste heat recovery," *Applied Thermal Engineering*,  
981 vol. 107, pp. 441-452, 2016.

- 982 [26] H. S. Pham *et al.*, "Mapping of the thermodynamic performance of the supercritical  
983 CO<sub>2</sub> cycle and optimisation for a small modular reactor and a sodium-cooled fast  
984 reactor," *Energy*, vol. 87, pp. 412-424, 2015.
- 985 [27] W. S. Jeong, J. I. Lee, and Y. H. Jeong, "Potential improvements of supercritical  
986 recompression CO<sub>2</sub> Brayton cycle by mixing other gases for power conversion system  
987 of a SFR," *Nuclear Engineering and Design*, vol. 241, no. 6, pp. 2128-2137, 2011.
- 988 [28] J.-E. Cha *et al.*, "Development of a supercritical CO<sub>2</sub> Brayton energy conversion  
989 system coupled with a sodium cooled fast reactor," *Nuclear Engineering and  
990 Technology*, vol. 41, no. 8, pp. 1025-1044, 2009.
- 991 [29] J. J. Sienicki *et al.*, "International collaboration on development of the supercritical  
992 carbon dioxide Brayton cycle for Sodium-cooled Fast Reactors under the Generation  
993 IV International Forum Component Design and Balance of Plant project," in  
994 *Proceedings of the 2010 International Congress on Advances in Nuclear Power  
995 Plants (ICAPP'10)*, San Diego, USA, pp. 392-399.
- 996 [30] A. Moisseytsev and J. J. Sienicki, "Investigation of alternative layouts for the  
997 supercritical carbon dioxide Brayton cycle for a sodium-cooled fast reactor," *Nuclear  
998 Engineering and Design*, vol. 239, no. 7, pp. 1362-1371, 2009.
- 999 [31] J. J. Sienicki, A. Moisseytsev, and L. Krajtl, "A Supercritical CO<sub>2</sub> Brayton Cycle  
1000 Power Converter for a Sodium-Cooled Fast Reactor Small Modular Reactor," in  
1001 *ASME 2015 Nuclear Forum collocated with the ASME 2015 Power Conference, the  
1002 ASME 2015 9th International Conference on Energy Sustainability, and the ASME  
1003 2015 13th International Conference on Fuel Cell Science, Engineering and  
1004 Technology*, 2015: American Society of Mechanical Engineers.
- 1005 [32] A. Dragunov, E. Saltanov, S. Bedenko, and I. Pioro, "A Feasibility Study on Various  
1006 Power-Conversion Cycles for a Sodium-Cooled Fast Reactor," in *2012 20th  
1007 International Conference on Nuclear Engineering and the ASME 2012 Power  
1008 Conference*, 2012, pp. 559-567: American Society of Mechanical Engineers.
- 1009 [33] J.-H. Eoh, H. C. No, Y.-B. Lee, and S.-O. Kim, "Potential sodium-CO<sub>2</sub> interaction of  
1010 a supercritical CO<sub>2</sub> power conversion option coupled with an SFR: Basic nature and  
1011 design issues," *Nuclear Engineering and Design*, vol. 259, pp. 88-101, 2013.
- 1012 [34] Y. Sun, Y. Zhang, and Y. Xu, "Study on coupling a gas turbine cycle to HTR-10 test  
1013 reactor," in *Proceedings of Technical Committee Meeting on Gas Turbine Power  
1014 Conversion Systems for Modular HTGRs*, Palo Alto, California (United States), 2000,  
1015 vol. IAEA-TECDOC-1238, pp. 42-51, Vienna, Austria: International Atomic Energy  
1016 Agency (IAEA), 2001.
- 1017 [35] N. Alpy *et al.*, "Gas cycle testing opportunity with ASTRID, the French SFR  
1018 prototype," in *Proceedings of Supercritical CO<sub>2</sub> Power Cycle Symposium*, Boulder,  
1019 Colorado (USA), 2011.
- 1020 [36] M. Saez, D. Haubensack, N. Alpy, A. Gerber, and F. Daid, "The use of gas based  
1021 energy conversion cycles for sodium fast reactors," in *Proceedings of the 2008  
1022 International Congress on Advances in Nuclear Power Plants-ICAPP'08*, Anaheim,  
1023 CA, 2008, Illinois, USA: American Nuclear Society, 555 North Kensington Avenue,  
1024 La Grange Park, 2008.
- 1025 [37] L. Cachon *et al.*, "Innovative power conversion system for the French SFR prototype,  
1026 ASTRID," in *Proceedings of the 2012 International Congress on Advances in Nuclear  
1027 Power Plants - ICAPP '12*, Chicago, IL, 2012, Illinois, USA: American Nuclear  
1028 Society, 555 North Kensington Avenue, La Grange Park, 2012.
- 1029 [38] French Alternative Energies and Atomic Energy Commission (CEA), "4th-Generation  
1030 sodium-cooled fast reactor: The ASTRID technological demonstrator," CEA Nuclear  
1031 Energy Division., Paris, 2012, Available:  
1032 [http://www.cea.fr/multimedia/Documents/publications/rapports/rapport-gestion-  
1034 durable-matieres-nucleaires/4th-generation-sodium-cooled-fast-reactors.pdf](http://www.cea.fr/multimedia/Documents/publications/rapports/rapport-gestion-<br/>1033 durable-matieres-nucleaires/4th-generation-sodium-cooled-fast-reactors.pdf),  
Accessed on: 10 November 2015.

- 1035 [39] P. P. Walsh and P. Fletcher, *Gas turbine performance*, 2nd ed. Oxford: John Wiley  
1036 and Sons, 2004.
- 1037 [40] J. Lee, J. I. Lee, Y. Ahn, and M. Choi, "Preliminary study of helium Brayton cycle  
1038 turbomachinery for small modular high temperature gas cooled reactor application,"  
1039 in *Proceedings of the 2013 International Congress on Advances in Nuclear Power  
1040 Plants (ICAPP'13)*, Jeju Island, Korea, 2013: Korea Nuclear Society.
- 1041 [41] V. Sobolev, "Database of thermophysical properties of liquid metal coolants for GEN-  
1042 IV," Belgian Nuclear Research Centre (SCK.CEN), Mol, Belgium, 2011, Available:  
1043 <http://hdl.handle.net/10038/7739>, Accessed on: 08 April 2015.
- 1044 [42] E. W. Lemmon, M. L. Huber, and M. O. McLinden, "NIST Standard Reference  
1045 Database 23: Reference Fluid Thermodynamic and Transport Properties-REFPROP,"  
1046 Version 9.1 ed. Gaithersburg: National Institute of Standards and Technology (NIST),  
1047 2013.
- 1048 [43] N. A. Carstens, "Control Strategies for Supercritical Carbon Dioxide Power  
1049 Conversion Systems," PhD Thesis, Massachusetts Institute of Technology (MIT),  
1050 Cambridge, Massachusetts, USA, 2007.
- 1051 [44] J. Floyd *et al.*, "A numerical investigation of the sCO<sub>2</sub> recompression cycle off-design  
1052 behaviour, coupled to a sodium cooled fast reactor, for seasonal variation in the heat  
1053 sink temperature," *Nuclear Engineering and Design*, vol. 260, no. 0, pp. 78-92, 2013.
- 1054 [45] J. C. Bryant, H. Saari, and K. Zanganeh, "An analysis and comparison of the simple  
1055 and recompression supercritical CO<sub>2</sub> cycles," in *Proceedings of Supercritical CO<sub>2</sub>  
1056 Power Cycle Symposium*, Boulder, Colorado (USA), 2011.
- 1057 [46] P. M. Fourspring and J. P. Nehrbaauer, "Heat exchanger testing for closed Brayton  
1058 cycle using supercritical CO<sub>2</sub> as working fluid," in *Proceedings of Supercritical CO<sub>2</sub>  
1059 Power Cycle Symposium*, Boulder, Colorado (USA), 2011.
- 1060 [47] S. A. Wright, M. E. Vernon, and P. S. Pickard, "Concept Design for a High  
1061 Temperature Helium Brayton Cycle with Interstage Heating and Cooling," Sandia  
1062 National Laboratories (SNL), Albuquerque, New Mexico and Livermore, California,  
1063 2006, Available:  
1064 [http://nuclear.inel.gov/deliverables/docs/genivihc\\_2006\\_milestone\\_report\\_7\\_1\\_2006  
1065 final.pdf](http://nuclear.inel.gov/deliverables/docs/genivihc_2006_milestone_report_7_1_2006_final.pdf).
- 1066 [48] R. K. Shah and D. P. Sekulic, *Fundamentals of heat exchanger design*. New Jersey:  
1067 John Wiley and Sons, 2003.
- 1068 [49] R. Le Pierres, D. Southall, and S. Osborne, "Impact of mechanical design issues on  
1069 printed circuit heat exchangers," in *Proceedings of Supercritical CO<sub>2</sub> Power Cycle  
1070 Symposium*, Boulder, Colorado (USA), 2011.
- 1071 [50] Q. Li, G. Flamant, X. Yuan, P. Neveu, and L. Luo, "Compact heat exchangers: A  
1072 review and future applications for a new generation of high temperature solar  
1073 receivers," *Renewable and Sustainable Energy Reviews*, vol. 15, no. 9, pp. 4855-4875,  
1074 2011.
- 1075 [51] J. E. Hesselgreaves, *Compact heat exchangers: selection, design and operation*.  
1076 Oxford (UK): Elsevier Science Ltd, 2001.
- 1077 [52] V. Dostal, M. J. Driscoll, and P. Hejzlar, "A supercritical carbon dioxide cycle for  
1078 next generation nuclear reactors," The MIT Centre for Advanced Nuclear Energy  
1079 Systems, Cambridge, Massachusetts (USA), MIT-ANP-TR-100, 2004, Available:  
1080 <http://web.mit.edu/22.33/www/dostal.pdf>.
- 1081 [53] S. J. Bae, J. Lee, Y. Ahn, and J. I. Lee, "Preliminary studies of compact Brayton cycle  
1082 performance for Small Modular High Temperature Gas-cooled Reactor system,"  
1083 *Annals of Nuclear Energy*, vol. 75, no. 0, pp. 11-19, 2015.
- 1084 [54] J. J. Sienicki, A. Moisseytsev, R. L. Fuller, S. A. Wright, and P. S. Pickard, "Scale  
1085 dependencies of supercritical carbon dioxide Brayton cycle technologies and the  
1086 optimal size for next-step supercritical CO<sub>2</sub> cycle demonstration," in *Proceedings of  
1087 Supercritical CO<sub>2</sub> Power Cycle Symposium*, Boulder, Colorado (USA), 2011.

- 1088 [55] Y. Gong, N. A. Carstens, M. J. Driscoll, and I. A. Matthews, "Analysis of Radial  
1089 Compressor Options for Supercritical CO<sub>2</sub> Power Conversion Cycles," Center for  
1090 Advanced Nuclear Energy Systems, MIT Department of Nuclear Science and  
1091 Engineering, and MIT Gas Turbine Laboratory of the Department of Aeronautics and  
1092 Astronautics., Cambridge, Massachusetts (USA), MIT-GFR-034, 2006, Available:  
1093 [http://nuclear.inl.gov/deliverables/docs/topical\\_report\\_mit-gfr-034.pdf](http://nuclear.inl.gov/deliverables/docs/topical_report_mit-gfr-034.pdf), Accessed on:  
1094 09 March 2014.
- 1095 [56] R. L. Fuller and W. Batton, "Practical considerations in scaling supercritical carbon  
1096 dioxide closed Brayton cycle power systems," in *Proceedings of Supercritical CO<sub>2</sub>*  
1097 *Power Cycle Symposium*, Troy, New York (USA), 2009.
- 1098 [57] O. Balje, *Turbomachines. A guide to Design, Selection and Theory*. New York: John  
1099 Wiley and Sons, 1981.
- 1100 [58] W. W. Bathie, *Fundamentals of gas turbines*, 2nd ed. New York: John Wiley and Sons,  
1101 1996.
- 1102 [59] R. S. R. Gorla and A. A. Khan, *Turbomachinery: design and theory*. New York:  
1103 Marcel Dekker Inc, 2003.
- 1104 [60] S. L. Dixon, *Fluid mechanics, thermodynamics of turbomachinery*, 5th ed. Oxford:  
1105 Elsevier Inc, 1998.
- 1106 [61] J. D. Mattingly, *Elements of gas turbine propulsion: Gas turbines and rockets*. Reston,  
1107 VA: American Institute of Aeronautics and Astronautics (AIAA), 2006.
- 1108 [62] H. I. H. Saravanamuttoo, G. F. C. Rogers, H. Cohen, and P. Straznicky, *Gas Turbine*  
1109 *Theory*, 6th ed. Essex (UK): Prentice Hall, Pearson Education, 2009.
- 1110 [63] J. Wang and Y. Gu, "Parametric studies on different gas turbine cycles for a high  
1111 temperature gas-cooled reactor," *Nuclear Engineering and Design*, vol. 235, no. 16,  
1112 pp. 1761-1772, 2005.
- 1113 [64] C. Wang, *Balance of Plant Analysis for High Temperature Gas Cooled Reactors:*  
1114 *Design and Optimization of Gas Turbine Power Conversion System, and Component*  
1115 *Design of Turbo-Machinery for Modular Pebble Bed Reactor Plants*. Saarbrücken  
1116 (Germany): Lambert Academic Publishing, 2009.
- 1117